Advances in Engineering Software 173 (2022) 103203

Contents lists available at ScienceDirect

Advances in Engineering Software

journal homepage: www.elsevier.com/locate/advengsoft

Application of metaheuristic optimization algorithms to evaluate the geometric and kinematic parameters of downbursts

Andi Xhelaj *, Massimiliano Burlando

Department of Civil, Chemical and Environmental Engineering, Polytechnic School, University of Genoa, Via Montallegro 1, Genoa 16145, Italy

ARTICLE INFO

Keywords:
Downburst analytical model
Metaheuristic algorithm
Differential evolution
Teaching-learning-based optimization
Single-objective optimization
Downburst kinematic parameters

ABSTRACT

Strong localized downbursts generated in thunderstorms can produce surface winds very dangerous for civil structures and infrastructures. Modelling and simulating such severe wind systems is therefore extremely important for structural safety and design wind speed evaluation. This paper deals with the downburst wind field simulation by means of an optimization algorithm that uses a downburst analytical model, previously developed by the authors, and two metaheuristic algorithms, namely the Differential Evolution (DE) and the Teaching-Learning-Based Optimization (TLBO), for the downburst kinematic and geometrical parameters evaluation. The optimization problem minimizes the relative error between recorded and simulated wind speed and direction time histories. A comparison is made between the performance of two algorithms for ten thunderstorm events measured in north-western Italy between October 2011 and October 2015. Both algorithms provide solutions which are coherent with the downburst parameters values present in literature. TLBO outperforms DE since it has a faster convergence rate to the optimal solution.

1. Introduction

The study of intense thunderstorm downbursts winds and their actions and effects on structures has been a dominant topic of the research in wind engineering over the last forty years [1]. Thunderstorms are non-stationary phenomena at the mesoscale, which occur in convective conditions with velocity profiles substantially different from those that are typical of the atmospheric boundary layer (ABL). Design wind velocities with mean return periods greater than 10-20 years are often associated with such phenomena [2]. Between the 1970's and 1980's Fujita made key contributions to the understanding of thunderstorms and their scales [3–6], showing that when the downdraft reaches the ground surface, it produces an intense radial outflow and ring vortices. Fujita called all these air movements "downburst" and divided these phenomena into "macroburst" and "microburst" depending on whether the outflow diameter is greater or smaller than 4 km, respectively [4]. Design wind speed and severe wind damage are often due to thunderstorm outflows, and they have a focal role in structural safety [1]. However, this matter is still affected by huge uncertainties and a shared model of downburst outflows and their actions on structures like the one formulated by Davenport [7] for synoptic cyclones is not available yet. The complexity of thunderstorms makes difficult to establish physically realistic and simple models of these phenomena. Downbursts have a short life cycle, and their small size enables a limited amount of data to be available. Downburst associated loads on structures, depend on a variety of parameters such as the diameter of the downdraft, the relative position between the center of the downburst and the structure, the translation velocity of the parent storm cell and so on. These aspects make the assessment of downburst wind loads very complex and require formulating simplified analytical or empirical models of this phenomenon able to capture their main features.

This study represents a natural continuation of a previous work concerning the reconstruction of the wind field produced during a downburst using an analytical model developed by the authors [8]. In the former work, the authors estimated the analytical model's parameters using a parametric approach that turned out to be too time-consuming and poorly efficient. This analysis was based on assigning a discrete set of values to each parameter in the analytical model and then calculate, for all combinations among the parameters, the relative error between anemometric measurements and simulated time histories of wind speed and direction. The combination corresponding to the lowest value of relative error was the one that led to match more closely the simulated downburst to the recorded data, and therefore was considered eligible for reconstructing the geometrical and

* Corresponding author.
E-mail address: andi.xhelaj@edu.unige.it (A. Xhelaj).

https://doi.org/10.1016/j.advengsoft.2022.103203
Received 15 February 2022; Received in revised form 20 June 2022; Accepted 23 July 2022
Available online 18 August 2022

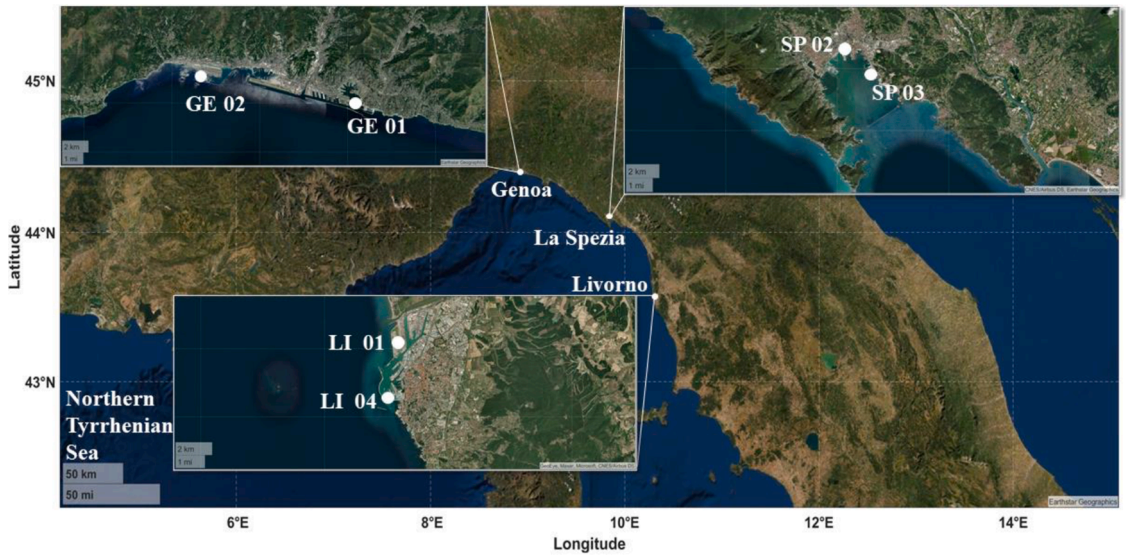

Fig. 1. The WP and WPS monitoring network used in this study. Geographic coordinates of the anemometers and their characteristics are reported in Table 1.

kinematical features of the downburst. However, the combination of, let's say, 10 parameters, each one having 10 different values, corresponds to 10^{10} relative errors that must be computed before evaluating the minimum, i.e. the final solution. This aspect considerably limited the use of this procedure to reconstruct a large number of thunderstorm-related downburst events. To overcome this shortcoming, in this paper the previous analytical model [8] is coupled with two global metaheuristic optimization algorithms, namely the Differential Evolution (DE) and the Teaching-Learning-Based Optimization (TLBO), with the purpose of determining the most efficient and reliable algorithm to solve the optimization problem related to the model's parameters identification. The algorithms are compared through the reconstruction of ten selected full-scale downburst events that occurred in the port area of La Spezia, Genoa and Livorno between October 2011 and October 2015.

This paper is organized into 6 Sections. Section 2 describe the full-scale measurements dataset used in the current study. Section 3 illustrates how the analytical model for simulating thunderstorm outflows is implemented and how the minimization problem is constructed starting from the definition of the objective function. Section 4 presents the implementation, and the pseudocodes of the two optimization algorithms, namely DE and TLBO. Section 5 presents the comparisons between the two proposed algorithm in the reconstruction of the space-time evolution of ten thunderstorm outflow events in the area of the High Tyrrhenian Sea. Section 6 summarizes the main conclusions and discuss prospects opened by this research.

2. Field measurements

The dataset of field measurements used in this paper originates from the two European Projects "Wind and Ports" (WP, 2009-2011) [9] and "Wind, Ports and Sea" (WPS, 2013-2015) [10,11]. Both projects were carried out by the Department of Civil, Chemical and Environmental Engineering (DICCA) of the University of Genova in cooperation with the harbor authorities of Genoa, Savona, La Spezia, Livorno and Bastia. One of the main objectives of these projects was to establish a statistical database on the various wind conditions in the Ligurian and Tyrrhenian Sea. In total, 28 ultrasonic anemometers (bi-axial and three-axial) have been installed across all ports. The sampling rate of the anemometers is 10 Hz (excluding the anemometers in Bastia, which have sampling rate of 2 Hz) and the anemometers have an accuracy of 0.01 m/s for wind speed and 1° for wind direction. Depending on the harbor, the elevation

Table 1
Main characteristics of the events considered and properties of the monitoring network.

Location	Date	Time (HH:MM: SS) UTC	Anemometer Code	Geographical Coordinates (λ, φ) (°N, °E)	Height AGL (m)	V_{max} (m/s)	$\overline{V}_{max}$ (m/s)	α (deg)
La Spezia	2011-10-25	15:40:00	SP 03	(44.097, 9.858)	10	37.12	26.53	187.8
	2012-04-11	07:10:00	SP 02	(44.110, 9.839)	13	24.2	18.46	221.3
	2012-04-19	12:50:00	SP 02	(44.110, 9.839)	13	25.64	16.6	210.3
	2012-10-15	00:20:00	SP 03	(44.097, 9.858)	10	24.23	19.69	241.1
	2014-07-25	06:20:00	SP 03	(44.097, 9.858)	10	22.3	15.8	289.3
Genoa	2012-09-30	21:00:00	GE 02	(44.418, 8.777)	13.3	21.53	17.1	163
	2012-10-28	06:20:00	GE 01	(44.399, 8.925)	61.4	26.8	22.6	162
Livorno	2012-10-01	12:10:00	LI 01	(43.570, 10.301)	20	18.91	15.66	268.1
	2015-09-13	11:00:00	LI 04	(43.541, 10.294)	20	24.08	19.34	333
	2015-10-04	05:10:00	LI 01	(43.570, 10.301)	20	29.46	19.15	347.1

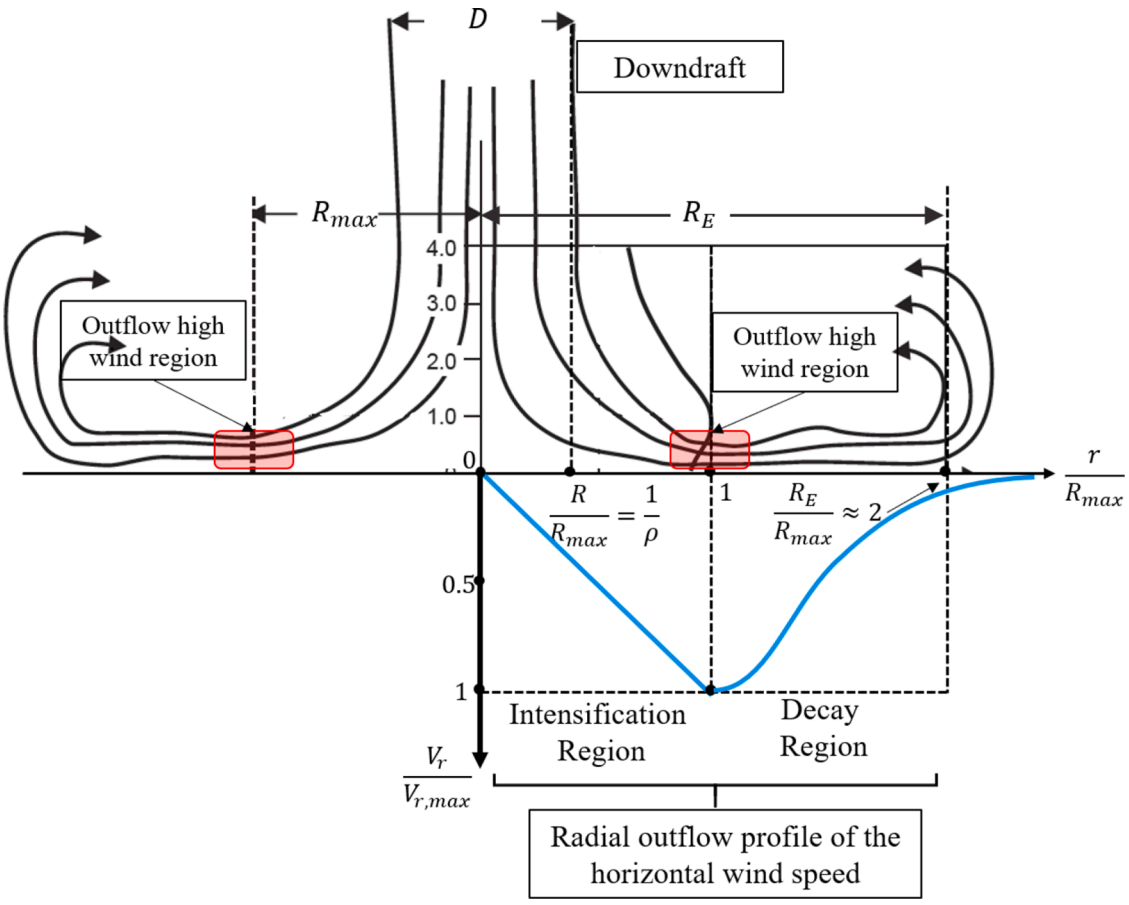

Fig. 2. Schematic view of a stationary downburst and outflow structure parameters. The horizontal wind velocity at height z AGL is characterized by radially symmetric streamlines with an annular ring of high winds (Adapted from [18]).

of the anemometers ranges from 10 to 75 m Above the Ground Level (AGL).

In the present article, ten episodes of non-stationary thunderstorm downburst events detected by the anemometers in the ports of La Spezia, Genoa and Livorno between October 2011 and October 2015 are examined. Fig. 1 depicts the locations of the anemometers within the port areas, whereas Table 1 reports the exact location of the anemometers and the main features of the downburst records analyzed in this document; the table includes the instantaneous peak wind velocity V_{max}, the maximum value of the slowly-varying mean wind velocity $\overline{V}_{max}$ (averaged over a 30 s moving window), and the wind direction α at the instant of peak velocityV_{max}.

The strongest event analyzed in this study was recorded in La Spezia with $V_{max} = 37.12$ m/s at 10 m AGL. It is worth noting that the direction α is merely indicative as it is the composition of thunderstorm outflow, storm motion and ABL flow [12]. Considering a translating downburst, the outflow direction detected by the sensor is the vectorial composition of the velocity and direction of the thunderstorm cell, treated as stationary, and its translational component [8]. The situation is complicated in the frequent case in which a thunderstorm cell is embedded into a background larger-scale boundary layer flow field, typically synoptic in nature. In principle all these cases may be handled as by vector superposition of the velocity and direction of flow components; however, there is no evidence that this approach is physically and mathematically appropriate. Xhelaj et al. [8] proposed in their analytical downburst model, as a first approximation, to continue adopting the vectorial superposition until a more realistic model won't be available in the literature. This strategy is used in the current work. As the model reported in Xhelaj et al. [8] is intended to provide the mean wind speed and direction only (i.e., turbulence is not included in this model), the single anemometer recordings of the 10 Hz-sampled horizontal wind speed and direction are decomposed, using a 30 second moving average window, into a slowly varying moving mean and a residual turbulent fluctuation, and only the slowly varying moving mean of the wind speed and direction is taken into consideration. The slowly varying mean wind speed, which for simplicity will henceforward be called $V(t)$, and the slowly varying mean wind direction, $\alpha(t)$, are retrieved according to the directional decomposition rule for thunderstorm outflows provided by Zhang et. al. [13]. Each time history record used in the actual work has a duration $\Delta t = 1$ hour [14] and is decomposed considering a moving average period $T = 30$ s [15,16]. Except for the La Spezia downburst of 2014-07-25, the remaining downbursts can be downloaded from the site of the THUNDERR project [17] database through the link http://portal.thunderr.eu/thunderview.

3. Model implementation

Section 3.1 describes the analytical model that simulates the mean horizontal wind speed and direction, evaluated at a generic point at fixed height z AGL, originating from a travelling downburst whose outflow is incorporated in a low-level, larger-scale ABL wind, generally of synoptic nature. An exhaustive description of the model is given in Xhelaj et al. [8]. However, for ease of reference, a short description is provided here. In Section 3.2, the objective function is defined, which is used later in the optimization procedure to calculate the model's parameters.

3.1. Thunderstorm outflow model

The primary hypothesis behind this model assumes that the

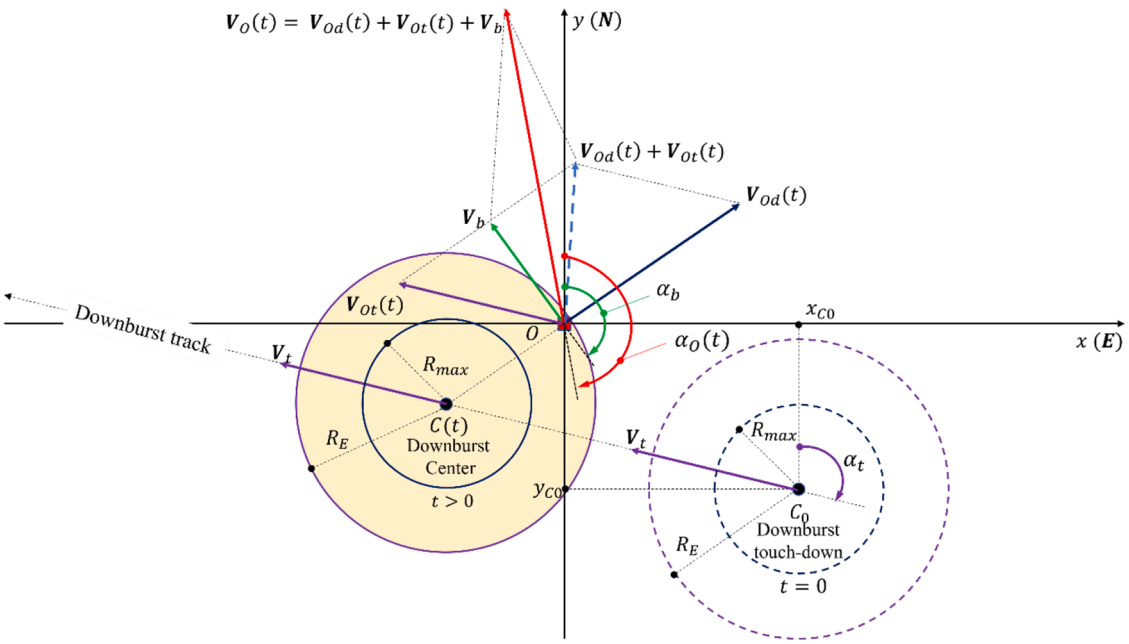

Fig. 3. Schematic representation of the translating downburst outflow embedded in and ABL background wind field according to the analytical model of Xhelaj et. al. [8].

combined wind speed and direction at a fixed elevation z which coincides with the location of a wind sensor or a structure is the vector sum of three independent velocity fields, namely the radial velocity of a spatially stationary downburst which is reconstructed according to a stream jet impinging orthogonally on a flat surface, the translation velocity due to the mean storm motion and the low level ABL mean wind velocity into which the downburst outflow near the surface is embedded.

In the initial modelling phase, it is assumed that the storm cell from which the downburst originates does not move relatively to the ground, thus the wind velocity field $\boldsymbol{V}_d$ of a non-translating downburst is considered [3,4]. In physical terms, a necessary requirement for this type of downburst is a calm wind environment (i.e., a very slow-moving storm and wind calm conditions within the atmospheric boundary layer). When the downdraft jet hits the ground, it starts to propagate with nearly symmetric outflows and a primary vortex ring of high wind velocity surrounds the downdraft core. Due to conservation of angular momentum the vortex ring at the base of the downdraft increases its vorticity and expands radially. The combination of the jet impingement and the stretching of the primary vortex ring largely increases the wind velocity, generating an outflow of high wind region which occurs approximately at a distance of two downdraft radii from the jet axis. The interaction between the primary vortex ring and the surface roughness can generate a secondary vortex ring near the leading edge of the primary ring.

Fig. 2 shows a schematic representation of the downburst and the parameters that describe the outflow structure, as adapted from Hjelmfelt [18]. Here, R represents the radius of the downdraft and it is assumed constant for the entire life cycle of the downburst, $R_{max}$is the radial distance from the downburst centre at which the maximum radial velocity ($V_{r,max}$) occurs, and R_E is the radial extension of the outer edge of the outflow (or gust front) from the downburst centre. Hjelmfelt [18] reported that, on average, when the downburst reaches maximum intensity, the extension of the outflow outer edge is approximately $R_E \approx 2R_{max}$. In Xhelaj et al. [8], the horizontal mean wind velocity at a fixed height z AGL due to a stationary downburst is reconstructed starting from a modification of the Holmes and Oliver model [19]. According to these authors, in the intensification region, $0 \le r \le R_{max}$, the horizontal radial velocity increases linearly with the radial distance from the stagnation point ($r = 0$) up to R_{max} where the maximum velocity occurs. In the decay region, $r > R_{max}$, an exponential decay of the horizontal radial velocity occurs. The position R_{max} depends linearly on R through the dimensionless parameter ρ which was assumed fixed and equal to 2 in Xhelaj et al. [8], while it is considered a decision variable and its value is determined by the optimization technique in this work. The model also incorporates an intensity-decay function that simulates the intensification and the decay of the downburst event on increasing the time as proposed by Chay at al. [20]. This function depends on T_{max}, which is the period of linear intensification from the initial simulation time ($t = 0$) to the maximum radial outflow intensity, while the total duration time is defined T_{end}.

Table 2
Model decision variables

1	Maximum radial velocity	$V_{r,max}$
2	Downdraft radius	R
3	Dimensionless radial distance from downburst center at which $V_{r,max}$ occurs	$\rho = \frac{R_{max}}{R}$
4	Period of linear intensification	T_{max}
5	Duration of the downburst event	T_{end}
6	x-component touchdown location (at$t = 0$)	x_{C0}
7	y-component touchdown location (at $t = 0$)	y_{C0}
8	Downburst translational velocity	V_t
9	Downburst translational direction	α_t
10	Low-level ABL wind speed	V_b
11	Low-level ABL wind direction	α_b

In the second modelling stage, the parent cloud producing the downburst is assumed to be in motion and embedded in a low level ABL flow (i.e., background flow). According to Fujita [3,4], due to the translation the front side of the storm intensify while the backside weakens, resulting in an asymmetric and strongly diverging directional flow. Also, the downburst wind near the surface is perturbed by the presence of the low-level ABL winds. Hjelmfelt [18,21] considered a linear interaction between these three-velocity fields and the main parameters that explain observed downburst events in terms of geometry and kinematics were retrieved by Hjelmfelt based on a linear interaction assumption. Accordingly, defining the translational velocity of the downburst cell $\boldsymbol{V}_t$and the low level ABL (i.e., background) wind $\boldsymbol{V}_b$, both

assumed constant for the life cycle of the downburst, the wind speed and direction in any points of the computational grid can be calculated as the vector sum of the three contributions $\boldsymbol{V} = \boldsymbol{V}_d + \boldsymbol{V}_t + \boldsymbol{V}_b$. In Fig. 3, the resulting wind velocity in position O is represented, while the downburst touch-down position at $t = 0$ is $C_0 = (x_{C0}, y_{C0})$. Here, a Cartesian reference system $x - y$ with the x-axis aligned towards the East and the y-axis aligned towards the North is used.

Table 2 summarizes the decision variables on which the Xhelaj et al. [8] model depends. They are necessary for the reconstruction of the thunderstorm events and consequently vary from case to case.

3.2. Objective function evaluation

The object of this analysis is to estimate the most appropriate value of the different field parameters that describe the downburst outflow. Table 2 provides a summary of the parameters on which the analytical model depends. The estimation of these parameters is performed (see Section 4) using global optimization algorithms.

Optimization problems can be founded in almost any scientific field. Real-world optimization problems are highly nonlinear, multimodal, discontinuous and under a variety of complicated constraints. This generally implies that the search for an optimal solution, or even a sub-optimal solution, is not a simple task. In the most general way, an optimization problem can be written as:

$$\begin{aligned} &minmize\ \boldsymbol{F}(\boldsymbol{X}) = (F_1(\boldsymbol{X}), \ldots, F_i(\boldsymbol{X}), \ldots, F_I(\boldsymbol{X})), \boldsymbol{X} = (X_1, X_2, \ldots, X_D) \in \Omega \subseteq \mathbb{R}^D \\ &subject\ to\ H_j(\boldsymbol{X}) = 0,\ (j = 1, 2, \ldots, J)\ G_k(\boldsymbol{X}) \le 0,\ (k = 1, 2, \ldots, K)\ X_d^{LB} \le X_d \le X_d^{UB}\ d = 1, 2, \ldots, D \end{aligned} \tag{1}$$

Problem (1) is called a multi-objective, nonlinear, constrained optimization problem; $\boldsymbol{X} = (X_1, X_2, \ldots, X_D) \in \Omega$ is the candidate solution with D decision variable parameters, $F_1(\boldsymbol{X}) \ldots F_I(\boldsymbol{X})$ are the objective functions, $H_j(\boldsymbol{X}) = 0$ denotes J equality constrained functions, $G_k(\boldsymbol{X}) \le 0$ represents K inequality constrained functions, and $X_d^{LB} \le X_d \le X_d^{UB}$ are D lower and upper bound constrains over the search space $\boldsymbol{X} \in \Omega \subseteq \mathbb{R}^D$. When $I = 1$, Problem (1) reduces to the standard form for a single-objective, nonlinear, constrained optimization problem. The simplest case of optimization is the single-objective ($I = 1$) unconstrained function optimization which means that both H_j and G_k are zero for each value of j and k. The current study deals with this type of optimization problems, which minimize a single objective function evaluated starting from simulations and recorded data.

Let $\boldsymbol{X} = \{X_i\}_{i=1}^{11} = \{V_{r,max}, R, \rho, T_{max}, T_f, x_{C0}, y_{C0}, V_t, \alpha_t, V_b, \alpha_b\}$ be the model decision variable vector which encapsulates the parameters of the model. The chosen objective function corresponds to the minimization of the relative error between the observed and the simulated slowly varying mean wind speed and direction. The relative error (RE) is used here for combining the wind speed error and the wind direction error. The RE, which is also the objective function, is given by:

$$F(\boldsymbol{X}) = F_{WS}(\boldsymbol{X}) + F_{WD}(\boldsymbol{X}) \tag{2}$$

where $F_{WS}(\boldsymbol{X})$ is the relative error between the magnitude of the simulated wind speed $V_O(t; \boldsymbol{X})$ at time t (Fig. 3) and the recorded wind speed $V(t)$at time$t$. $F_{WD}(\boldsymbol{X})$ is the relative error between the simulated wind direction $\alpha_o(t; \boldsymbol{X})$ at time t (Fig. 3) and the recorded wind direction $\alpha(t)$ at time t.

While is relatively easy to evaluate the $F_{WS}(\boldsymbol{X})$, the same cannot be said for the $F_{WD}(\boldsymbol{X})$ since the wind direction is a circular data and to evaluate $F_{WD}(\boldsymbol{X})$ some concepts of circular statistics are needed. In order to evaluate $F_{WS}(\boldsymbol{X})$, let $\boldsymbol{V_O}(\boldsymbol{X}) = \{V_{O1} V_{O2} \ldots V_{ON}\}$ be the set of the simulated wind speed data at the observing point O in $\Delta t = 1$ h and let $\boldsymbol{V} = \{V_1 V_2 \ldots V_N\}$ be the set of the recorded slowly varying wind speed data in $\Delta t = 1$ h. N is the total sample of simulated wind speed data present in 1 h. Since the simulation time step in this work is $\Delta t_S = 1$ s, then $N = 3600$ samples. The Relative Error between the simulated and the observed wind speed data is given by (see the Appendix for more detail on its derivation):

$$F_{WS}(\boldsymbol{X}) = \frac{\sum_{i=1}^{N} (V_{Oi}(\boldsymbol{X}) - V_i)^2}{\sum_{i=1}^{N} V_i^2} \tag{3}$$

To evaluate the Relative Wind Direction Error $F_{WD}(\boldsymbol{X})$, let $\boldsymbol{\alpha_O}(\boldsymbol{X}) = \{\alpha_{O1} \alpha_{O2} \ldots \alpha_{ON}\}$ be the set of the simulated wind direction data in $\Delta t = 1$ h and let $\boldsymbol{\alpha} = \{\alpha_1 \alpha_2 \ldots \alpha_N\}$ be the set of the recorded slowly varying wind direction data in $\Delta t = 1$ h. According to the theory of circular statistics is possible to show that the Relative Error between the simulated and the observed wind direction is given by (see the Appendix A for more details on its derivation):

$$F_{WD}(\boldsymbol{X}) = \frac{2}{N} \cdot \sum_{i=1}^{N} \{1 - cos(\alpha_{Oi} - \alpha_{Oi}(\boldsymbol{X}))\} \tag{4}$$

After the definition of the objective function the decision variables are found by solving the following minimization problem:

$$\begin{aligned} &Minnimize\ F(\boldsymbol{X}),\ X = \{X_1, X_2, \ldots, X_D\} \in \Omega \subseteq \mathbb{R}^D \\ &subjected\ to\ X_d^{LB} \le X_d \le X_d^{UB}\ d = 1, 2, \ldots, D = 11 \end{aligned} \tag{5}$$

Problem (5) represents a single-objective, nonlinear and bound constrained optimization problem and represents a special case of Problem (1). The minimization problem has $D = 11$ number of decision variable parameters and each parameter have its variable bounds which ultimately defines the search space $\Omega \subseteq \mathbb{R}^D$ where the minimization must be performed. The minimization process in this study was carried out for each of the ten events presented in Table 1. The solution of each optimization problem allows to estimate the model parameters $\boldsymbol{X}$. The knowledge of these parameters ultimately allows to reconstruct the bi-dimensional slowly varying mean wind field at the height of the anemometer/structure and therefore to come up with the simulated time history of the slowly varying mean wind speed and direction. Appendix B provides a detailed analysis of the fact that the uncertainty associated with the anemometric measurements has no impact on the uncertainties associated with the model predictions.

It is worth noting that the minimization process has the main goal to globally minimize the objective function F. The information about the derivative of F is impractical since the computation capacity is limited. The two-metaheuristic methods used in the current study, described in the following sections, proved being able to provide a sufficient good solution to the global optimization problem in hand given the incomplete information and the limited resource capacity.

4. Optimization algorithm implementation

To solve Problem (5), efficient optimization algorithms are necessary. In the current work metaheuristic optimization algorithms are considered for the solution of the minimization problem. All modern nature-inspired algorithms are called metaheuristic [22,23]. The word

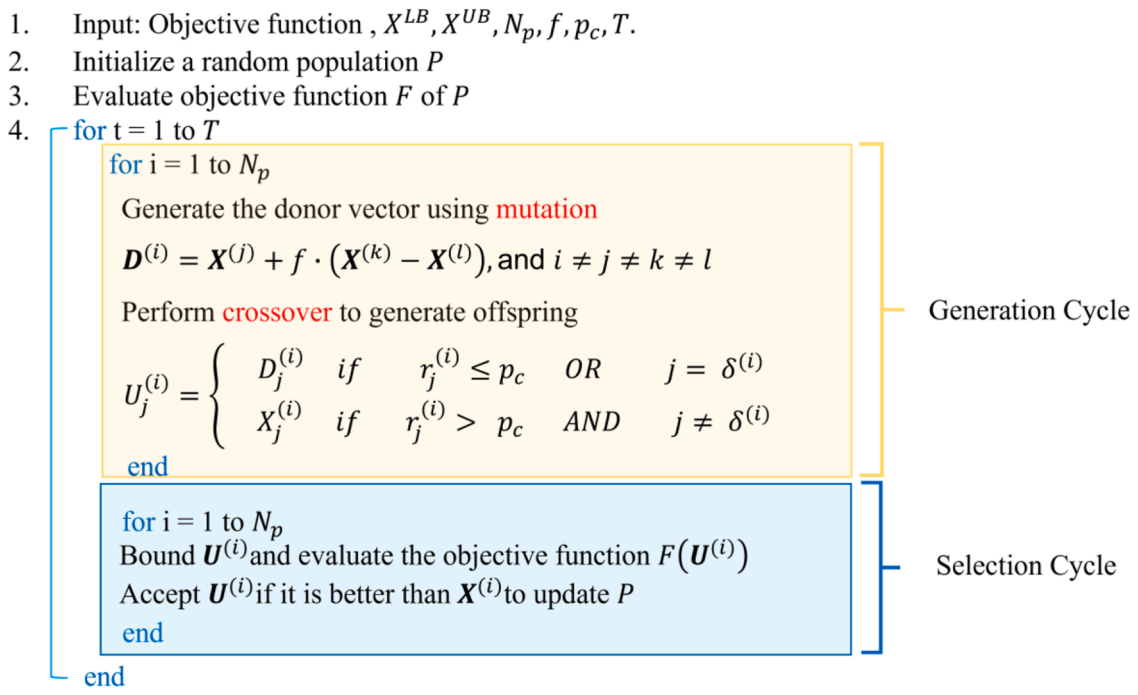

Fig. 4. Pseudocode of the Differential Evolution Algorithm.

"metaheuristic" was coined by Glover [23], and it is referred to higher-level procedure or heuristic designed to find, generate, or select a heuristic that may provide a sufficiently good solution to an optimization problem [24]. Optimization algorithms that employ metaheuristic methods constitute a modern approach in the scientific method of optimization. The first big step in this direction comes with the advent of evolutionary algorithms. Between the 1960s and 1970s Holland [25] developed the Genetic Algorithms (GAs). GAs are stochastic population-based and many new evolutionary algorithms that have developed since then have strong similarities to genetic algorithms. Metaheuristic algorithms underwent a broad development in the 1980s and 1990s. Two important algorithm developed in that period were simulated annealing (SA) by Kirkpatrick et al. [26] and Tabu search [27]. SA is a trajectory-based algorithm technique of finding a global optimum solution in a very vast search space. Tabu search is a local search method and is the first algorithm in metaheuristic that makes uses of memory structures to avoid previous visited solutions. In the 1990s two global optimization algorithms based on swarm intelligence emerged. Dorigo [28] developed a population-based algorithm called Ant Colony Optimization (ACO), which was inspired by the swarm intelligence of social ants. Kennedy and Eberhart [29] developed the Particle Swarm Optimization (PSO), which was inspired by the natural behavior of flocks of birds or insects swarming. In the beginning of the 21st century, the development of new metaheuristic algorithm has intensified dramatically. Most of them are based on a metaphor of some natural or man-made process. Geem et al. developed the harmony search [30] algorithm in 2001, which is a music inspired algorithm and belongs to the class of evolutionary algorithm. In 2005, Karaboga developed the artificial bee colony algorithm (ABC) which is inspired by the foraging behaviour of bees [31]. In 2009, Yang and Deb introduced an efficient cuckoo search (CS) algorithm [32]. Many new metaheuristic algorithms are still emerging today and there is no doubt that more metaheuristic algorithms and new application will emerge in the future.

In the following section two metaheuristics optimization techniques are considered for the minimization problem (5), namely the Differential Evolution (DE) and the Teaching Learning Based Optimization (TLBO) algorithms. Both algorithms are used for global search optimization since they are stochastic, and population based. Differential evolution (DE) [33] has gained increasing attention for solving optimization problems in many scientific and engineering fields. DE belongs to the category of evolutionary algorithms. The algorithm can be considered a further development of genetic algorithms. Unlike GAs, differential evolution carries out operations over each component or each dimension of the solution. DE requires a set of parameters to be specified by the user which remain invariant during the iterations. Since DE is population based, the user should specify the population size (i.e., the set of agents), cross over probability, amplification factor and also stopping criterion. The stopping criterion in the current study is defined as the total number of iterations that the algorithm will have to perform.

TLBO was recently proposed by [34]. The inspiration for this algorithm is a knowledge transfer in a classroom environment. The algorithm constitutes in two phases. Considering a classroom environment, the teaching usually happens in two phases. One is the Teacher Phase and the second is the Learner Phase. In the first phase the teacher interacts with the students training to increase their knowledge. In the second phase the students interacting among themselves try to further increase their knowledge. TLBO mimics these two phases. Unlike DE, TLBO requires as user specified parameter only the population size and the stopping criterion.

Although there is a vast choice of metaheuristic technique currently present in the literature, the choice of TLBO and DE was made mainly based on the number of internal parameters that each algorithm has and whose calibration is very important in order to obtain a good result in terms of convergence of the objective function. Since in the analytical model $D = 11$ parameters have to be determined through the objective function, it does not seem appropriate to use metaheuristic methods depending on a large number of internal parameters. For example, the classic PSO and the real coded GA have respectively 5 and 6 internal parameters to be calibrated case by case, which increases the difficulty in finding an optimal solution a lot. This is because in addition to the parameters of the analytical model, it is also necessary to determine the parameters of the optimization algorithm. From this point of view, TLBO has only 2 internal parameters, which are common to all meta-heuristic algorithms, while DE presents 4 internal parameters to be determined (i.e., population size, stopping criterion, cross over probability and amplification factor).

1. Input: Objectice function, $\boldsymbol{X}^{LB}, \boldsymbol{X}^{UB}, N_p$, T
2. Initialize a random population $[P]$
3. Evaluate objective function F of $[P]$
4. for t = 1 to T

for i = 1 to N_p

Choose $\boldsymbol{X}_{teacher}$

Determine $\boldsymbol{X}_{mean}$

$\boldsymbol{X}_{new}^{(i)} = \boldsymbol{X}^{(i)} + \boldsymbol{R}.* \left(\boldsymbol{X}_{teacher} - T_F \cdot \boldsymbol{X}_{mean}\right)$

Bound $\boldsymbol{X}_{new}^{(i)}$ and evaluate the objective function $F\left(\boldsymbol{X}_{new}^{(i)}\right)$

Accept $\boldsymbol{X}_{new}^{(i)}$ if it is better than $\boldsymbol{X}^{(i)}$

Teacher Phase

Choose any solution randomly, $\boldsymbol{X}^{(p)}$ with p ≠ i

Determine $\boldsymbol{X}_{new}^{(i)}$ as:

If $F\left(\boldsymbol{X}^{(i)}\right) < F\left(\boldsymbol{X}^{(p)}\right)$

$\boldsymbol{X}_{new}^{(i)} = \boldsymbol{X}^{(i)} + \boldsymbol{R}.* \left(\boldsymbol{X}^{(i)} - \boldsymbol{X}^{(p)}\right)$

else

$\boldsymbol{X}_{new}^{(i)} = \boldsymbol{X}^{(i)} - \boldsymbol{R}.* \left(\boldsymbol{X}^{(i)} - \boldsymbol{X}^{(p)}\right)$

end

Bound $\boldsymbol{X}_{new}^{(i)}$ and evaluate the objective function $F\left(\boldsymbol{X}_{new}^{(i)}\right)$

Accept $\boldsymbol{X}_{new}^{(i)}$ if it is better than $\boldsymbol{X}^{(i)}$ to update $[P]$

Learner Phase

end

end

Fig. 5. Pseudocode of the Teaching-Learning Based Optimization Algorithm

Section 4.1 and 4.2 provide the generic implementation of the two metaheuristics algorithms, TLBO and DE as well as their corresponding pseudocodes.

4.1. Implementation of the differential evolution algorithm

Considering the minimization problem defined in Section 3.3 by Eq. (5) a population matrix of *Np* solutions vectors $\boldsymbol{X}^{(i)}, i = 1, 2, \ldots, Np$ is generated using uniformly distributed random numbers within the domain of decision variables. The size of the population matrix *Np* is decided by the user. Each solution is called target vector and is described by the following notation: $\boldsymbol{X}^{(i)} = (X_1^{(i)}, X_2^{(i)}, \ldots, X_D^{(i)})$, where $D = 11$ are the decision variable parameters. Differential Evolution consists mainly of three main operations: mutation, crossover, and selection.

In the mutation operation, the algorithm randomly chooses three distinct vectors from the population matrix, $\boldsymbol{X}^{(j)}, \boldsymbol{X}^{(k)}$, and $\boldsymbol{X}^{(l)}$, and then generates the so-called donor vector by the following mutation scheme:

$$\boldsymbol{D}^{(i)} = \boldsymbol{X}^{(j)} + f \cdot \left(\boldsymbol{X}^{(k)} - \boldsymbol{X}^{(l)}\right) \textbf{with} i, j, k, l = 1, 2, \ldots, N_p \textbf{and} i \neq j \neq k \neq l \quad (6)$$

In Eq. (6) the parameter *f* is called amplification factor and should be defined by the user. This parameter controls the amplification of the differential variation $(\boldsymbol{X}^{(k)} - \boldsymbol{X}^{(l)})$. In principle, $f \in [0, 2]$, but in practice, a scheme with $f \in [0.5, 1]$ is more efficient and stable [35]. Altogether four vectors are involved in the mutation of the target vector $\boldsymbol{X}^{(i)}$ and therefore the population size of the DE algorithm should be $N_p \geq 4$.

The crossover operation is controlled by the crossover probability $p_c \in [0, 1]$ which should be decided in the begging of the algorithm by the user. The crossover scheme can be carried out in two ways: binomial and exponential. In the current work the binomial crossover scheme is adopted. The later performs crossover on each of the *D* components of the donor vector $\boldsymbol{D}^{(i)}$ and the target vector $\boldsymbol{X}^{(i)}$ and generates the trial vector $\boldsymbol{U}^{(i)}$ according to the following operation:

$$U_j^{(i)} = \begin{cases} D_j^{(i)} \ if \ \ r_j^{(i)} \leq p_c \ OR \ j = \ \delta^{(i)} \\ X_j^{(i)} \ if \ r_j^{(i)} > \ p_c \ AND \ j \neq \ \delta^{(i)} \end{cases} \quad j = 1, 2 \ldots, D \quad (7)$$

where, $U_j^{(i)}$ is the *j*-th component of the trial vector $\boldsymbol{U}^{(i)}$; $D_j^{(i)}$ is the *j*-th component of the donor vector $\boldsymbol{D}^{(i)}$ and $X_j^{(i)}$ is the *j*-th component of the target vector $\boldsymbol{X}^{(i)}$. Moreover, $r_j^{(i)} = rand\ (0, 1)$ is a uniform random number on the interval [0, 1] and independently generated for each component *j* and for each solution *i*; $\delta^{(i)} = randint(1, D)$ is an integer randomly chosen from 1 to *D* and newly generated for each solution *i*.

If the trial vector violates the bounds of the decision variable parameters, it is necessary to bound the new solution in the following manner:

$$U_j^{(i)} = \begin{cases} min\left\{U_j^{(i)}, X_j^{UB}\right\} \ if \ U_j^{(i)} \geq X_j^{UB} \\ max\left\{U_j^{(i)}, X_j^{UB}\right\} \ if \ U_j^{(i)} \leq X_j^{LB} \end{cases} \quad j = 1, 2, \ldots D \quad (8)$$

Once the algorithm has generated all the N_P trial vectors, then a greedy selection strategy is employed between the target vector and the trial vector. Population is than updated:

$$\boldsymbol{X}_{new}^{(i)} = \begin{cases} \boldsymbol{U}^{(i)} \ if \ F\left(\boldsymbol{U}^{(i)}\right) < F\left(\boldsymbol{X}^{(i)}\right) \\ \boldsymbol{X}^{(i)} \ if \ F\left(\boldsymbol{U}^{(i)}\right) \geq F\left(\boldsymbol{X}^{(i)}\right) \end{cases} \quad (9)$$

Whichever vector is better or whichever solution has the lowest objective function value will survive and update the population. The above procedure must repeat multiple times because this is the generalized structure of metaheuristic techniques. The procedure is stopped after the maximum number of iterations *T* is reached. *T* is the user-defined parameter which should be fixed by the user in the beginning of procedure.

The pseudocode for DE is shown in Fig. 4.

The basic DE/Rand/1/Bin scheme is carried out in this work, but at least 10 different schemes have been formulated. For more detail on this topic, refer to Price et al. [36].

4.2. Implementation of the teaching learning based optimization algorithm

As in the case of DE, the user should define a population matrix of *Np*

solutions vectors $\boldsymbol{X}^{(i)}$,$i = 1, 2, \ldots, Np$ generated using uniformly distributed random numbers within the domain of decision variables of the minimization problem. In TLBO the population size indicates the number of students, and the decision variable parameters indicates the subjects offered in the class. The TLBO learning process is divided into main stages: Teacher phase and Learner phase. In the first phase a new solution is generated with the help of the teacher solution and the mean of the population. Assume $X^{(i)} = (X_1^{(i)}, X_2^{(i)}, \ldots, X_D^{(i)})$ is the position of the i-th solution (student) in the population, the learner with the least objective function value is identified as a teacher $\boldsymbol{X}_{teacher} = \boldsymbol{X}_{f(\boldsymbol{X})=min}$ and the mean position of the class with N_P learners can be expressed as $\boldsymbol{X}_{mean} = N_P^{-1} \cdot \sum_{i=1}^{N_P} \boldsymbol{X}_i$. Once the teacher solution and the mean solution are evaluated, the position of current i-th learner $\boldsymbol{X}^{(i)}$ which undergoes teacher phase is updated by the following equation:

$$\boldsymbol{X}_{new}^{(i)} = \boldsymbol{X}^{(i)} + \boldsymbol{R}. * (\boldsymbol{X}_{teacher} - T_F \cdot \boldsymbol{X}_{mean}) \tag{10}$$

$\boldsymbol{R} = rand(0, 1, [1, D])$is a random 1-by-D vector which elements are uniformly distributed within [0, 1] and the symbol .* indicates an elements by elements multiplication. $T_f = randint(1, 2)$ is an integer random number, called the teaching factor, it has to be either 1 or 2. Before evaluating the objective function of the new solution, it is important to ensure that the new solution does not violates the lower and the upper bound of the decision variables. The objective function is to be evaluated only for the solution within the bounds. If the new solution violates the bounds than it is necessary to bound the new solution in the following manner:

$$X_{new,j}^{(i)} = \begin{cases} min\left\{X_{new,j}^{(i)}, X_j^{UB}\right\} \text{ if } X_{new,j}^{(i)} \geq X_j^{UB} \\ max\left\{X_{new,j}^{(i)}, X_j^{UB}\right\} \text{ if } X_{new,j}^{(i)} \leq X_j^{LB} \end{cases} j = 1, 2, \ldots D \tag{11}$$

Once the new solution is within the bound of the decision variables, the objective function of the new solution is evaluated. After this step, a greedy selection is performed to update the population:

$$\boldsymbol{X}_{new}^{(i)} = \begin{cases} \boldsymbol{X}_{new}^{(i)} \text{ if } F\left(\boldsymbol{X}_{new}^{(i)}\right) < F\left(\boldsymbol{X}^{(i)}\right) \\ \boldsymbol{X}^{(i)} \text{ if } F\left(\boldsymbol{X}_{new}^{(i)}\right) \geq F\left(\boldsymbol{X}^{(i)}\right) \end{cases} \tag{12}$$

If $F(\boldsymbol{X}_{new}^{(i)}) < F(\boldsymbol{X}^{(i)})$, the new solution enters the population in place of the old solution which was used to generate it otherwise the new solution will be discarded and the old solution will be maintained.

In the second phase a new solution is generated starting from the current solution $\boldsymbol{X}^{(i)}$, with the help of a partner solution. The partner's solution is a randomly selected solution from the population matrix. Let the partner solution be $\boldsymbol{X}^{(p)}$, with p being an integer number randomly chosen between 1 and Np and $p \neq i$. The new solution evaluated in the learning process can be expressed by the following equation:

$$\boldsymbol{X}_{new}^{(i)} = \begin{cases} \boldsymbol{X}^{(i)} + R. * \left(\boldsymbol{X}^{(i)} - \boldsymbol{X}^{(p)}\right) \text{ if } F\left(\boldsymbol{X}^{(i)}\right) < F\left(\boldsymbol{X}^{(p)}\right) \\ \boldsymbol{X}^{(i)} - R. * \left(\boldsymbol{X}^{(i)} - \boldsymbol{X}^{(a)}\right) \text{ if } F\left(\boldsymbol{X}^{(i)}\right) \geq F\left(\boldsymbol{X}^{(p)}\right) \end{cases} \tag{13}$$

where $F(\boldsymbol{X}^{(i)})$ is the objective function value of the current solution, $F(\boldsymbol{X}^{(p)})$ is the objective function value of the auxiliary solution It is worthy of note that TLBO does not require any user-defined parameter for the Teacher phase and the Learner phase, thus making the implementation of TLBO much simpler than DE. Again, the newly generated solution in the learner phase $\boldsymbol{X}_{new}^{(i)}$ must undergo corner bounding, expressed by Eq. (11), and after that the objective function of the new solution is evaluated, and a greedy selection strategy is performed as described by Eq. (12). If $\boldsymbol{X}_{new}^{(i)}$ is better than the current solution $\boldsymbol{X}^{(i)}$, $\boldsymbol{X}_{new}^{(i)}$ is used to replace $\boldsymbol{X}^{(i)}$, otherwise the old solution $\boldsymbol{X}^{(i)}$ is maintained and the new solution $\boldsymbol{X}_{new}^{(i)}$ is discarded.

The above procedure must be repeated multiple times and it is stopped after the maximum iteration number T is achieved. T is the user-defined parameter which is fixed in the beginning of the procedure.

The pseudocode for TLBO is shown in Fig. 5.

Table 3
Upper and lower bound of 4 parameters as reported by Wilson et al. [38].

1	Maximum radial velocity	$V_{r,max}(m/s)$	6*to*18.5
2	Downdraft radius*	$R(m)$	500*to*1650
3	Radial distance at which $V_{r,max}$ occurs	$R_{max}(m)$	750*to*3350
4	Period of intensification at which $V_{r,max}$ occurs	$T_{max}(min)$	~ 2 *to* 28

* The downdraft radius is assumed by the authors of the current paper to coincide approximately with the distance from the downburst center where the radial velocity $V_r \geq 2$ m/s.

It is noteworthy that the original version of TLBO by Rao et al. [34] employed a duplicate removal strategy. In the current work the duplicate removal strategy was not employed since the probability to have two duplicate solutions is very low. For more information on the TLBO algorithm refer to Rao [37].

5. Simulation results and comparisons of differential evolution with teaching learning based optimization

In this section, in order to compare the two proposed algorithms (Section 4), ten different real scale downbursts events occurred in the port areas of La Spezia, Genoa and Livorno between October 2011 and October 2015 are examined. The geographic position of the three port areas and the anemometer locations that recorded these events are given in Fig. 1, while the main characteristics of each downburst event are briefly described in Table 1. These ten events are simulated solving the Xhelaj et al. [8] analytical model with the two optimization algorithms, namely the DE and TLBO algorithms. The application of these algorithms to the downburst model is performed through the definition of the optimization Problem (5) described in Section 3, and its implementation as reported in Section 4. Since Problem (5) represents a single-objective, nonlinear and bound constrained optimization problem, the user should define carefully, according to the physics of the problem in hand, the lower and the upper bound of the $D = 11$ decision variable parameters which ultimately defines the search space $\Omega \subseteq \mathbb{R}^D$ where the optimization should be performed. This is done in Section 5.1. In order to do a fair comparison between the two algorithms, it is important that the simulation sittings are the same for both the algorithms. Moreover, as explained in Section 4.2 the implementation of the DE is more difficult with respect to TLBO, since the choice of the user defined parameter in DE can have a large effect on optimization performance. The common simulation settings for both of the algorithms and the tuning of the parameters for the DE algorithm are presented in Section 5.2. The comparison between the algorithms is based on the performance of each algorithm in finding a reasonably good optimal solution of Problem (5) for each of the ten test-cases, given the incomplete information provided by the objective functions and the limited resource capacity. The metric to evaluate the algorithms efficiency is based on the convergence behaviour of the objective function towards the best solution as the number of iterations increases. Section 5.3 discusses the comparisons of the two algorithms in the case of the ten downbursts event present in the current study.

Table 4
Upper and lower bound of 7 parameters as reported by Hjelmfelt [18].

1	Maximum radial velocity	$V_{r,max}(m/s)$	6*to*21
2	Downdraft radius	$R(m)$	600*to*1550
3	Radial distance at which $V_{r,max}$ occurs	$R_{max}(m)$	1000*to*3500
4	Period of intensification at which $V_{r,max}$ occurs	$T_{max}(min)$	2*to*16
5	Duration of the downburst event, from intensification to decay	$T_{end}(min)$	8.1*to*31.4
6	Downburst translation velocity	V_t	4*to*8
7	Low-level ABL wind speed	V_b	3*to*11

Table 5
Summary of dimensionless radial position of maximum horizontal velocity.

Authors	$\rho = R_{max}/R$	Comments
Hjelmfetl (1988) [18]	1.7	From full scale measurements
Chay et al. (2006) [20]	2 to 2.5	From computational fluid dynamics
Kim and Hangan [40]	2.2	From numerical simulations of steady and unstedy impinging jets
Xu and Hangan (2008) [41]	2.2	From experimental investigation
Mason et al. (2011) [42]	2.5	From numerical simulation using the cooling approach

Table 6
Lower and upper bound of the decision variable parameters for the optimization Problem (15).

1	Maximum radial velocity	$V_{r,max}(m/s)$	$0to40$
2	Downdraft radius	$R(m)$	$200to2000$
3	Dimensionless radial distance from downburst center at which $V_{r,max}$ occurs.	$\rho = \frac{R_{max}}{R}\ (-)$	$1.6to2.6$
4	Period of linear intensification	T_{max}(min)	$2to15$
5	Duration of the downburst event	T_{end}(min)	$15to45$
6	x-component touchdown location (at $t = 0$)	$x_{C0}(m)$	$-10000to10000$
7	y-component touchdown location (at $t = 0$)	$y_{C0}(m)$	$-10000to10000$
8	Downburst translational velocity	$V_t\ (m/s)$	$0to40$
9	Downburst translational direction	α_t(deg)	$0to359.9$
10	Low-level ABL wind speed	$V_b\ (m/s)$	$0to40$
11	Low-level ABL wind direction	α_b(deg)	$1\ to359.9$

5.1. Definition of the lower and upper bound of decision variable parameters

Dealing with thunderstorm downburst events, it is important to carefully define the lower and the upper bound of the decision variable parameters (Table 2), as is expected for the solution of Problem (5). To give a reasonable lower and upper bound of the decision variable parameters, the authors performed a literature review on the values of these parameters. In the following, a selection of some relevant scientific contributions on this matter is reported.

Table 3 summarises the main findings from Wilson et. al [38], who reported some parameters based on radar reconstruction of the space and time scale of 38 downburst events extracted during the Joint Airport Weather Studies (JAWS, 1982) Project [39].

According to Wilson et. al [38], the average maximum radial velocity was 12 m/s. The average downburst radius was 900 m and the average radial distance from the downburst center when the maximum radial velocity occurs was 1550 m; consequently, on average the dimensionless parameter $\rho = R_{max}/R$ is equal to $\rho = 1.70$. Lastly the average period of intensification at which $V_{r,max}$ occurs was 6.4 mins, and 95 % of the downbursts reached maximum intensity before 10 minutes. It should be noted that in [38], the intensification time starts when the radial velocity $V_r \geq 5$ m/s, this means that the time the downburst passes from zero to the maximum radial velocity $V_{r,max}$ is grater than the data provided by Wilson et al. [38].

Table 4 summarises the main finding from Hjelmfelt [18], again based on radar reconstruction of 27 downburst events extracted from the JAWS Project. In this work, Hjelmfelt [18] reanalyze some cases already studied by Wilson et al [38].

According to the study carried out by Hjelmfelt [18], the average maximum velocity was 12 m/s. The average downburst radius was 900 m and the average radial distance from the downburst center when the maximum velocity occurs was 1550 m; These results confirm the observation carried out by [38]. However, the average period of intensification at which $V_{r,max}$ occurs was 7.8 minutes, and ~95% of the downbursts reached maximum intensity before 15 minutes. The mean duration of the entire downburst event was ~ 16 minutes. It is worthy of note that the starting and the decay phase of the downburst event is measured when the radial velocity V_r is larger than zero, which means that the event itself has a slight longer life cycle that the data given by Hjelmfelt [18]. In the wind engineering practice, when dealing with thunderstorm downbursts, an important parameter that plays a major role on design and safety of structures with respect to the actions of downburst winds, is the dimensionless radial position of the maximum velocity $\rho = R_{max}/R$. Table 5 summarizes the values of ρ that can be found in literature.

According to the performed literature review, the lower and upper bounds for the optimization Problem (15) were chosen as reported in Table 6. The simulation space domain for the downburst is an area of 20 × 20 km^2 and the grid size in x and y direction is 50 m. The station that records the passing of the downburst is located at the center of this domain. Downburst can come from any direction; hence the translation direction ranges from 0° to 359.9°. The same holds for the low-level ABL wind direction.

Table 7
Algorithms' parameters setting for DE and TLBO.

Algorithm	Parameter setting
Common settings (both DE and TLBO)	Population size: $N_P = 110$ Maximum iterations: $T = 500$ Problem dimension: $D = 11$ Number of independent runs = 256 Average time for a single simulation ~ 30 minutes
DE	Amplification factor: $f = 0.85$ Cross over probability: $p_c = 0.8$

5.2. Computer configuration and algorithm's parameters settings

All the simulations in the current study were performed in MATLAB R2020a (serial computing) on a 64-bit Windows 10 Home Edition with Intel i7 (7th Gen) central processing unit (4 cores) at 3.20 GHz and 16 GB of RAM. According to the structure of the pseudocodes given in Section 4, both the algorithms can run in parallel, using all the available core resources, which considerably reduces the computational time. In order to properly compare the performance of algorithms, the simulation settings should be the same for both of them. As already said, TLBO algorithms require only the specification of the population size and the maximum number of iterations for the termination criteria, whereas DE requires also the amplification factor f and the crossover probability p_c. The choice of the right population size is very important in all metaheuristic methods, because if the population size is too small there will be not enough diversification, too few solutions will explore the search space and the algorithm will most probably converge prematurely towards a basin of attraction of a local minimum. A good rule of thumb in metaheuristic is to use a population size $N_P = 10*D$ [35]. Since $D = 11$, the populations size for both the algorithms is N_P=110. The number of maximum iterations for both algorithms is $T = 500$. Since both DE and TLBO are stochastic in nature the algorithms are run independently 256 times in order to achieve a best solution, this choice allows both of the algorithms to explore more deeply the search space and to avoid getting stuck in local optimal regions. The choice of DE parameters $f \in [0, 1]$ and $p_c \in [0, 1]$ can have a large impact on the optimization performance [35, 36]. According to Zaharie [43], who carried out a mathematical convergence analysis concerning these parameters selection, in order to obtain a good convergence as the number of iterations increases the factor c, defined below, should be greater than 1:

Table 8
Algorithm convergence results for 256 independent runs in terms of best, mean and Std for the ten downburst events in the port areas of La Spezia, Genoa and Livorno.

Optimization Problem			DE Algorithm			TLBO Algorithm		
Location	Date	Code	Best	Mean	Std	Best	Mean	Std
La Spezia	2011-10-25	S1	0.4462	0.4518	0.0024	**0.4440**	**0.4469**	**0.0061**
	2012-04-11	S2	0.3681	0.3742	0.0033	**0.3597**	**0.3623**	**0.0038**
	2012-04-19	S3	0.3367	0.3369	0.0001	**0.3362**	**0.3365**	**0.0005**
	2014-07-25	S4	0.1112	**0.1148**	0.0029	**0.1108**	0.1266	**0.0392**
	2014-07-25	S5	0.6647	0.6846	0.0090	**0.6419**	**0.6746**	**0.0598**
Genoa	2012-09-30	G1	0.3549	0.3583	0.0017	**0.3487**	**0.3494**	**0.0038**
	2012-10-28	G2	0.3027	0.3032	0.0027	**0.2939**	**0.2996**	**0.0293**
Livorno	2012-10-01	L1	0.0669	0.1216	0.0169	**0.0531**	**0.1214**	**0.0304**
	2015-09-13	L2	0.0675	0.0777	0.0016	**0.0647**	**0.0772**	**0.0254**
	2015-10-04	L3	0.2547	0.3201	0.0308	**0.2204**	**0.2851**	**0.0978**

$$c = 2{\cdot}f^2{\cdot}p_c - 2{\cdot}\frac{p_c}{N_P} + \frac{p_c^2}{N_P} + 1 > 1$$

Considering the suggestion given by Storn [35] that a good choice of the amplification factor and the crossover probability are respectively $f \in [0.5, 1]$ and $p_c \in [0.8, 1]$, preliminary tests were performed to determine suitable f and p_c values to adopt in all the optimization problems. According to this preliminary analysis, the values of amplification factor f= 0.85 and crossover probability $p_c = 0.8$ were chosen, which correspond to $c = 1.47 > 1$ for the Zaharie's condition. This combination of parameters gave the best results in terms of convergence in the case of the DE algorithm for all the 10 cases investigated in the current work. With the above settings, the average time for a downburst simulation was $\sim$ 30 minutes.

Table 7 presents the parameters setting of each algorithm.

5.3. Simulation and result comparisons for ten downburst events in the port area of La Spezia, Genoa and Livorno

In the current section, the results of ten downburst events that occurred in the port area of La Spezia, Genoa and Livorno (Table 1) are reported. The location of the anemometers that captured these ten downburst events are given in Fig. 1.

A brief meteorological survey and weather scenarios of the thunderstorm occurred in the port area of La Spezia in 2012-04-11 is given in Xhelaj et al. [8], while the event that occurred in 2011-10-25 is described in Burlando et al. [14]. Considering the port area of Genoa, again a meteorological survey of the downburst occurred on 2012-09-30 is given in Xhelaj et al., [8]. As far as the port area of Livorno is concerned, a brief weather scenario of the downburst event occurred on 2015-09-13 is given in [12], while, a very detailed meteorological survey and weather scenarios analysis on the thunderstorm occurred on 2012-10-01 is provided by [15].

The simulation (reconstruction) procedure is carried out by finding a reasonably good solution of the optimization Problem (15). For each case the optimization procedure is performed using the DE and the TLBO algorithms. To avoid distinguishing each downburst event (i.e., optimization problem) by the location and the date, a code was given to each problem as shown in Table 8. Results are then compared together in order to determine which algorithm performs better. For the algorithms parameters setting refer to Table 7. The metric for evaluating the algorithm's performance is mainly based on the convergence behavior of the objective function value towards the best solution. More specifically, the comparison metrics are based on the best, mean and standard deviation (Std) objective function value of the 256 independent runs that both algorithms reach after 500 iterations. The best objective function value, or the best solution, represents the lowest value reached by the 256 independent runs after 500 iterations (i.e., the best optimum solution of the optimization problem). The mean objective function value gives information about the overall performance of the 256 runs after 500 iterations. If the average value approaches the best solution, all the 256 independent runs converge approximately to the best solution achieved by the algorithm. However, there is no guarantee that the best solution coincides with the global minimum of the optimization problem. The Std value of the 256 objective functions after 500 iterations describes the amount of variation or dispersion from the mean value of these runs. Without however knowing the nature of the best solution provided by the algorithm, that is, whether the algorithm reaches a global or local

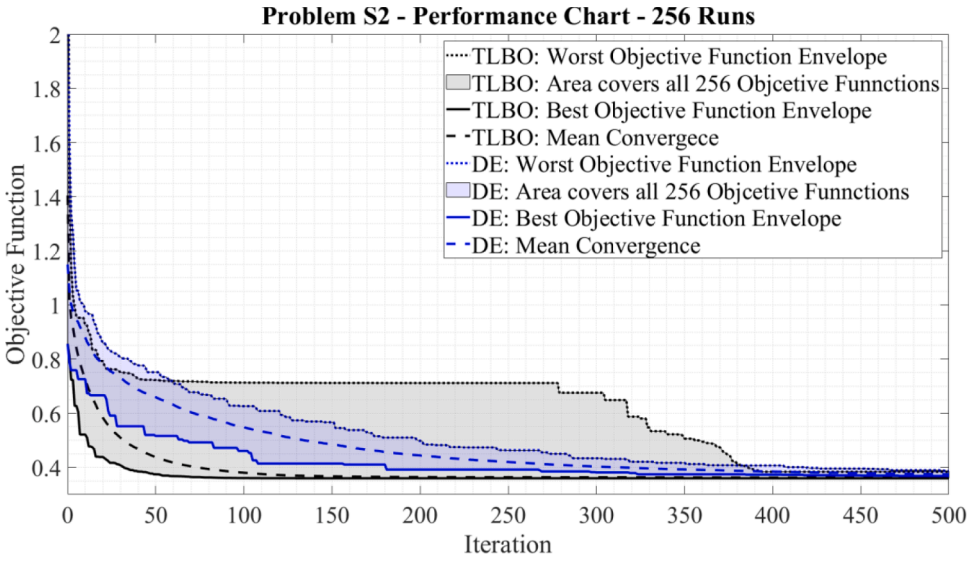

Fig. 6. Performance chart for the Problem S2, representative of the first group comprised of cases S1, S2, G1, L1 and L3.

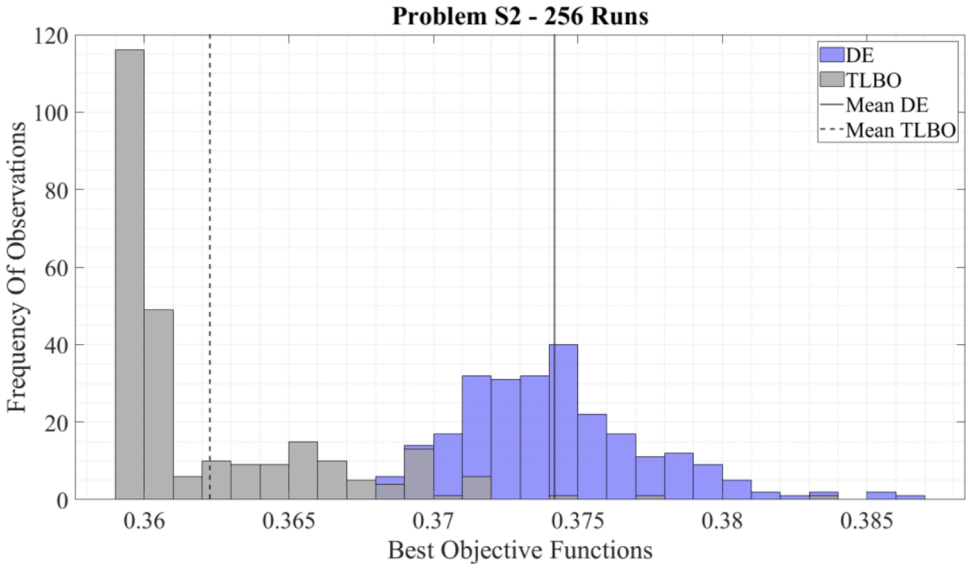

Fig. 7. Frequency of the observations (histogram) of the 256 best objective function values relative to Problem S2, representative of the first group comprised of cases S1, S2, G1, L1 and L3.

minimum, then a high variability of the standard deviation of the 256 best objective functions is an indicator that the algorithm explores the search space more deeply and therefore finds more optimal solutions to the problem.

The best solution, the mean and the Std value that both algorithms reach after 500 iterations for the ten cases examined in the current work are given in Table 8.

As can be noted from Table 8 in all ten downbursts cases, the algorithm that has better convergence values both in the best solution and in the mean value of all the solutions (highlighted in bold) is the TLBO, with the exception of the mean value of case S4.

At the same time TLBO presents for all the ten cases a bigger Std (highlighted in bold) than DE. As for cases S1, S2, G1, L1 and L3 the Std values achieved with TLBO are higher than DE but nevertheless they have the same order of magnitude, while for cases S3, S4, S5, G2 and L2 the Std values are one order of magnitude bigger in TLBO than in DE. This indicates that, for the problem in hand, TLBO finds more optimal solutions than DE.

To further describe the performance of both algorithms in a more quantitative fashion, two representative cases of the ten total cases are considered.

The first case is representative of the group containing the cases S1, S2, G1, L1 and L3, where the Std values achieved with TLBO are higher than DE but still have the same order of magnitude. For this purpose, the case S2 is considered as representative of the first group.

The second case is representative of the group containing S3, S4, S5, G2 and L2 where the Std values evaluated with TLBO are one order of magnitude bigger than DE. S5 is chosen as representative of the second group.

Fig. 6 shows the "performance charts" for the case S2 (refer to Table 8 for the downburst identification) which is representative of the first group.

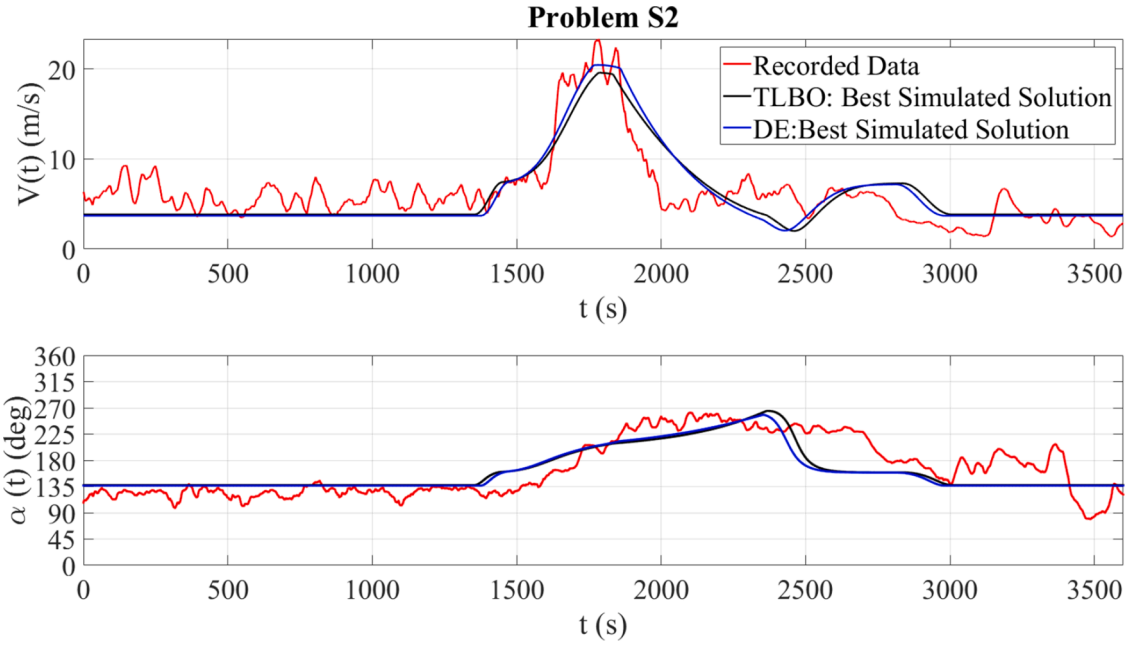

Fig. 8. Simulation results (in terms of slowly varying wind speed (top) and direction (bottom) for the Problem S2.

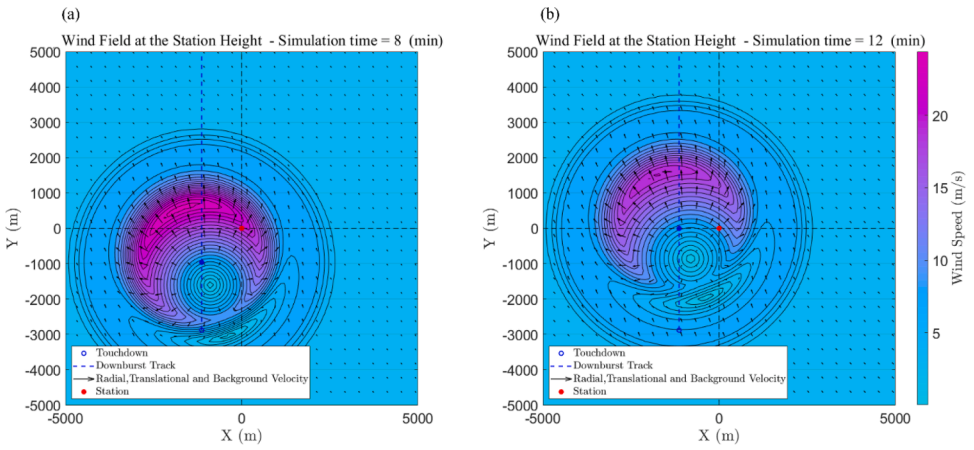

Fig. 9. Downburst wind field reconstruction for the Problem S5 using the overall best solution achieved with the TLBO algorithm. (a) Downburst reconstruction at simulation time = 8 minutes; (b) Downburst reconstruction at simulation time = 12 minutes. The red dot indicates the position of station/anemometer and coincides with the origin O of the reference frame, the blue circle indicates the downburst center relative to the simulation time. The blue dashed line indicates the downburst path.

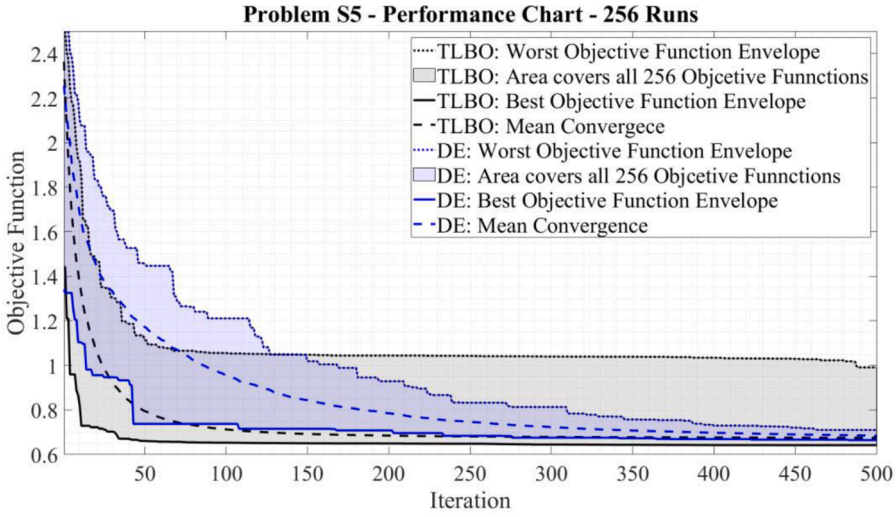

Fig. 10. Performance chart for the Problem S5, representative of the second group comprised of cases S3, S4, S5, G2, and L2.

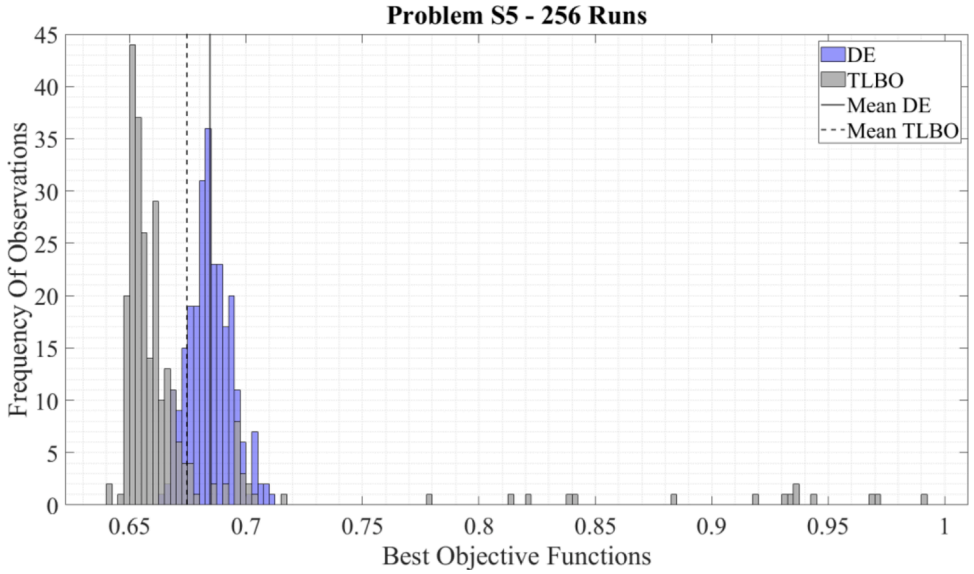

Fig. 11. Frequency of the observations (histogram) of the 256 best objective function values relative to Problem S5, representative of the first group comprised of cases S3, S4, S5, G2, and L2.

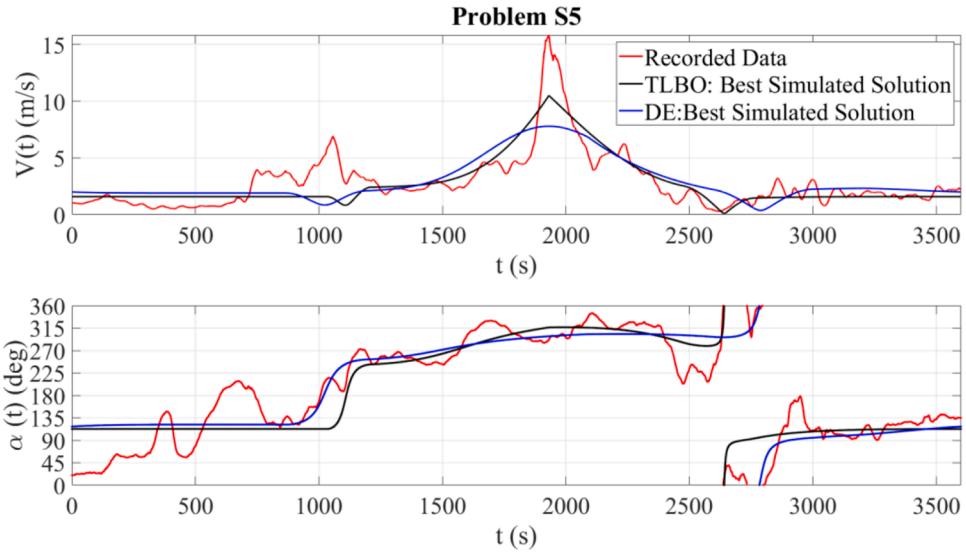

Fig. 12. Simulation results (in terms of slowly varying wind speed (top) and direction (bottom-) for the Problem S5.

The performance chart describes for both the algorithms the convergence of the objective functions as the number of iterations increases. This chart contains the upper and lower envelope of all the 256 convergence curves. The area between the lower and upper envelope contains within it the trend of the objective function values for all the 256 independent runs as the number of iterations increases. Obviously at the end of the 500 iterations, the value of the upper envelope coincides with the worst objective function value (worst solution) while the lower envelope coincides with the best objective function value (best solution) that both the algorithms have found. In the performance chart it is traced (dashed line) for both the algorithms the mean convergence curve as the number of iterations increases for the 256 independent runs. The analysis of the performance charts shows an important characteristic of the two algorithms, which can be crucial for reducing the computational time in pseudo-operational applications of this model. In fact, in all of the five cases belonging to the first group, the lower envelope curve and the mean convergence curve associated with TLBO have much lower values than the DE counterpart, except when they get closer to the maximum iteration number. The two curves reach almost stable values after 50 to 100 iterations for TLBO, which indicates that TLBO convergences at a much faster rate than DE (almost 1 order of magnitude, i.e. ~50 against ~500). The rate of convergence of the algorithms is a very important element when comparing algorithms, because it allows to reduce the computation cost by reducing the maximum number of iterations (stopping criterion). This fact becomes very relevant, in particular, when dealing with the simulation (or optimization) of a large number of downburst events.

Fig. 7 shows for the case S2, representative of the first group, the frequency of the observations (histogram) of the 256 best objective function values

The Fig. shows the position of the mean for both the algorithms and explains also why the TLBO has a slightly greater value of the Std with respect to DE. The histogram of TLBO revels that TLBO is capable of detecting some solution which are far from the mean value. The presence of these outlier solutions increases the Std of TLBO with respect to DE, which demonstrates its greater flexibility in exploring the search space of the parameters.

Fig. 8 shows for the problem S2, the time history of the overall best simulation results (i.e., the one that produce the lowest objective function), in terms of slowly varying mean wind speed (top) and direction (bottom) for both the algorithms, compared to the recorded data.

The Fig. show in a qualitative way the goodness of fit between simulations and full-scale measurements. Both algorithms give very similar best results, as expected according to their corresponding objective function values reported in Table 8.

Fig. 9 shows the downburst wind field reconstruction and evolution for the Problem S2 using the overall best solution achieved with the TLBO algorithm. The slowly varying downburst mean wind field is

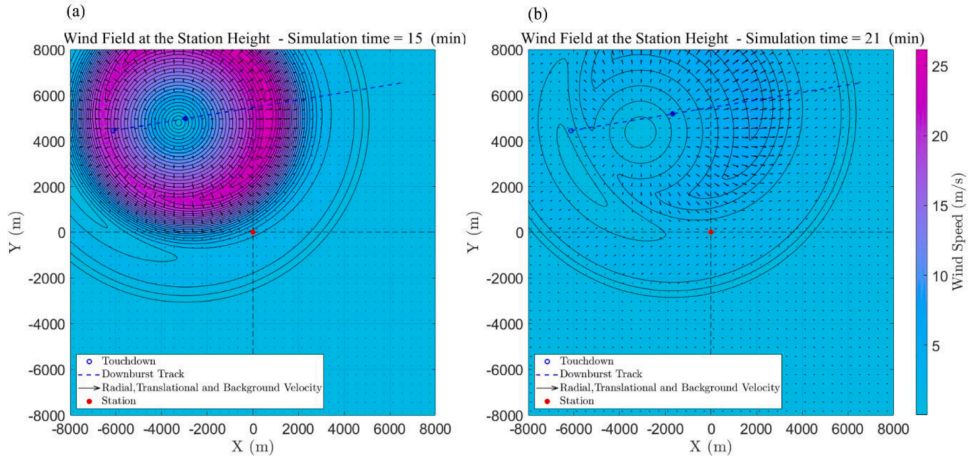

Fig. 13. Downburst wind field reconstruction for the Problem S5 using the overall best solution achieved with the TLBO algorithm. (a) Downburst reconstruction at simulation time = 15 minutes; (b) Downburst reconstruction at simulation time = 21 minutes. The red dot indicates the position of station/anemometer and coincides with the origin O of the reference frame, the blue circle indicates the downburst center relative to the simulation time. The blue dashed line indicates the downburst path.

Table 9
TLBO & DE best simulations results. Downburst parameters for the ten downburst events in the port area of La Spezia, Genoa and Livorno. Solutions related to DE are given in parentheses.

	TLBO & (DE) - Best Solution - Decision Variable Parameters										
Code	$x_{C0}(m)$	$y_{C0}(m)$	$R(m)$	$\rho(-)$	$V_{r,max}(m/s)$	T_{max}(min)	T_{end}(min)	$V_t(m/s)$	α_t(deg)	V_b (m/s)	α_b(deg)
S1	-126.79	-1288.23	350.00	1.80	15.92	4.77	30.76	3.51	169.56	7.54	168.15
	(-292.57)	(-1357.61)	(356.48)	(1.88)	(16.02)	(4.30)	(27.81)	(3.94)	(177.14)	(7.59)	(167.19)
S2	-1135.60	-2884.44	650.00	2.48	17.12	8.00	40.00	4.00	180.00	3.83	137.45
	(-1071.34)	(-2767.71)	(648.69)	(2.48)	(19.94)	(8.07)	(29.81)	(4.02)	(179.45)	(3.69)	(136.50)
S3	1611.28	827.17	950.00	2.40	25.98	15.00	21.67	7.00	160.49	7.30	220.61
	(1669.69)	(802.85)	(889.99)	(2.40)	(25.67)	(14.94)	(23.22)	(6.52)	(159.52)	(7.35)	(220.75)
S4	-4278.99	-839.46	1452.29	1.98	15.64	3.04	25.93	4.53	230.05	4.66	123.61
	(-4032.95)	(-876.01)	(1743.19)	(1.98)	(15.81)	(3.06)	(25.95)	(4.35)	(228.66)	(4.55)	(124.76)
S5	-6127.60	4442.67	1509.33	2.34	23.78	15.00	24.08	3.58	260.61	1.58	112.51
	(-7131.21)	(2542.29)	(1150.76)	(2.41)	(24.03)	(11.06)	(33.36)	(3.57)	(274.90)	(1.89)	(121.38)
G1	-433.53	-3034.62	579.05	2.50	16.97	11.12	27.00	2.40	210.46	2.54	19.25
	(-545.59)	(-2708.73)	(493.32)	(2.46)	(16.81)	(12.75)	(29.45)	(2.03)	(211.38)	(2.30)	(20.10)
G2	1054.36	-11.36	999.98	2.14	18.27	10.00	20.34	6.56	170.00	14.79	174.15
	(1124.16)	(42.88)	(1099.03)	(2.02)	(19.92)	(10.76)	(18.67)	(6.69)	(170.00)	(14.82)	(174.31)
L1	-463.33	877.56	744.84	2.06	14.55	13.08	28.58	1.98	40.82	3.16	357.45
	(-694.52)	(1272.46)	(1122.89)	(2.04)	(16.28)	(13.01)	(25.89)	(2.81)	(35.87)	(3.30)	(359.60)
L2	-4718.21	5268.21	1699.58	2.40	25.43	4.01	22.15	5.68	309.39	6.73	179.50
	(-4127.32)	(4185.79)	(1514.45)	(2.33)	(28.56)	(4.15)	(23.34)	(4.12)	(308.69)	(6.63)	(177.56)
L3	537.17	6061.05	1499.49	2.36	23.78	8.83	30.38	4.42	330.97	3.53	194.63
	(251.08)	(5147.39)	(1360.68)	(2.16)	(27.19)	(6.60)	(29.44)	(4.01)	(330.47)	(2.74)	(201.16)
Mean values			1043.46	2.25	19.74	9.29	27.09	4.37	213.30*	5.57	154.32*
			(1037.95)	(2.22)	(21.02)	(8.87)	(26.69)	(4.21)	(217.93)*	(5.49)	(155.68)*
Standard deviations			468.31	0.24	4.46	4.38	5.80	1.65	1.36 (1.38)	3.83	1.19 (1.18)
			(445.56)	(0.22)	(4.95)	(4.22)	(4.21)	(1.44)		(3.88)	

* Mean value and Std are evaluated using circular statistics

reconstructed at the height of the station where the original downburst signal was recorded (refer to Table 1 for the actual anemometer height above the ground level). Fig. 9 (a) captures the downburst phenomena at the time of its maximum intensification, which for the current case is 8 minutes, while Fig. 9 (b) shows the downburst during its decay phase, 4 minutes after the maximum intensification.

Fig. 10 shows the "performance charts" for the case S5 (refer to Table 8 for the downburst identification) which is representative of the second group.

Also, for the second group, with the exception of the case S3, the lower envelope curve associated with TLBO presents lower values than the DE counterpart, except when they get closer to the maximum iteration number, which again indicates that TLBO converges faster than DE.

Fig. 11 shows for the case S5, representative of the second group, the frequency of the observations (histogram) of the 256 best objective function values.

The Fig. shows the position of the mean for both the algorithm. TLBO in this case explore more deeply the search space in the neighbourhoods of the mean position as is evident from the presence of more outlier solutions which are farther from the mean value. The frequent presence of the outlier solutions describes therefore the reason why the Std deviation of TLBO is for the second group nearly one order of magnitude greater than the corresponding DE. Therefore, outliers are here responsible for the larger variance of TLBO distribution. Conversely, DE produces a more compact cluster of solutions that are similar with each other, while TLBO produces a wider cluster or more than one cluster of solutions which in principle could be different from each other. This last feature is desirable because the existence of more optimal solutions indicates that the data provided in input by the objective function (i.e., the recorded slowly varying mean wind speed and direction) is in some circumstances not really enough to overall understand the downburst which took place and consequently more data is needed for the correct reconstruction of the real physical phenomenon. Having however several solutions to the problem in hand and gathering supplemental information regarding the downburst to be simulated, such as Radar/LiDAR or Satellite data, it is therefore possible to decrease the amount of uncertainty by choosing the correct solution which is also consistent with the supplemental data.

Fig. 12 shows for the problem S5, the time history of the overall best simulation results (i.e., the one that produce the lowest objective function), in terms of slowly varying mean wind speed (top) and direction (bottom) for both the algorithms, compared to the recorded data. The Fig. presents some detachment from the recorded wind speed. A reason for this detachment is due to the fact that the La Spezia site (refer to Fig. 1) has a complex orography and can substantially perturb the downburst outflows. This aspect is not included in the analytical model yet. However, as far as the wind direction is concerned, there is a very good correlation between recoded and simulated data.

Fig. 13 shows the downburst wind field reconstruction and evolution for the Problem S5 using the overall best solution achieved with the TLBO algorithm. The slowly varying downburst mean wind field is reconstructed at the height of the station where the original downburst signal was recorded (refer to Table 1 for the actual anemometer height above the ground level). Fig. 13 (a) captures the downburst phenomena at the time of its maximum intensification, which for the current case is 15 minutes, while Fig. 13 (b) shows the downburst during its decay phase, 6 minutes after the maximum intensification.

Table 9 shows the value of the parameters that produced the best overall solution using TLBO and DE algorithms for the ten downburst events. The values of these parameters allow to reconstruct the downburst time-space evolution through the analytical model for each of the ten cases as is seen in the Fig. 9 and 13. The two algorithms produce always very similar results, highly correlated to the experimental measurements, which confirms the ability of the minimization problem to carefully match the temporal profiles of the observed data. Table 9 also reports, except for the touch-down locations that would be meaningless, the mean and the Std values of these parameters for the ten cases considered. These values, that are produced from both the algorithms, are coherent with the mean values currently found in the literature and reported in Section 5.1.

6. Conclusions and prospects

This paper proposes a comparison between two metaheuristic optimization algorithms, namely the Differential Evolution (DE) and the

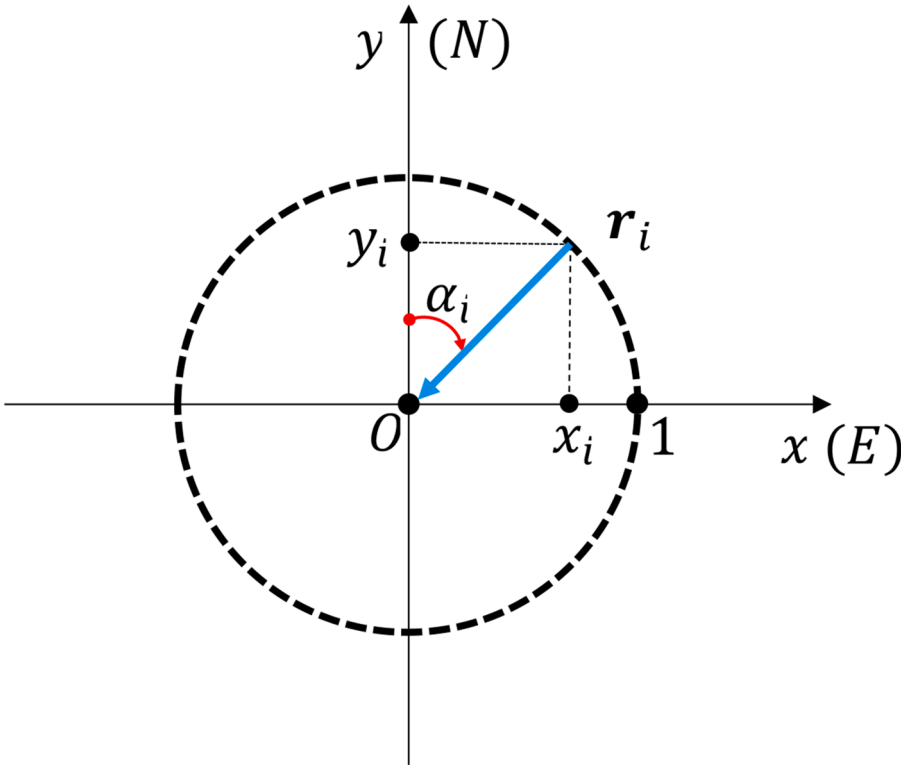

Fig. A1. Polar to rectangular mapping: $\alpha_i \Leftrightarrow \boldsymbol{r}_i = (x_i, y_i)$

Teaching-Learning-Based Optimization (TLBO), which are used to evaluate the parameters of the Xhelaj et al. [8] downburst model, applied to ten full-scale downburst events. The analysis of the performance of the two algorithms for the 10 optimization problems considered led to the following conclusions:

- TLBO is easier to use than DE, as it only requires the population number and the maximum number of iterations as input, while DE, in addition, requires also defining the amplification factor f and the crossover probability p_c. Differential evolution performance is closely linked to the choice of these two parameters which should be calibrated by the user which inevitably leads to a higher computational time when using the DE algorithm.
- The numerical results of the objective functions, in terms of best, mean and std obtained for the ten cases, show that TLBO has always better performance in terms of best ad mean result, while DE for all the ten cases has a lower std value than TLBO. The later suggest that TLBO explores more deeply the search space than DE.
- The convergence analysis for the ten cases considered reveals that TLBO outperforms DE. TLBO has a faster convergence rate than DE, which makes TLBO more efficient since it is possible to reduce the computational cost.
- The results of both algorithms provide, when the best solution is considered, a very good match between the observed and simulated time histories of slowly varying mean wind speed and direction.
- The wind field reconstruction for the ten downburst cases using TLBO and DE as optimization algorithms provides decision value parameters, associated to the best solution, which are coherent with the values present in literature.

It is worth noting that the result obtained by both the algorithms depends mostly on the definition of the objective function and the search space. In fact, in the current work it is used only the information given by one anemometer that records the passage of the downburst event. Clearly, if more anemometers measure the same event, this new information could be incorporated in the definition of the objective function. For example, staying in the realm of single-objective function minimization, it will be possible to define the objective function as the sum of relative errors for different anemometers. This new information can greatly enhance the robustness of the optimization procedure results. Analogously, the optimization procedure could be made more robust using different kind of meteorological data, e.g., Radar or LiDAR measurements, which is expected to narrow the range of variation of the parameters hence reducing further the search space.

In perspective, as the TLBO algorithm turned out to be fast-performing and accurate enough for its application as an optimization technique to the Xhelaj et al. [8] downburst model, this result pave the way to the application of the model in two different ways. On the one hand, a wide catalogue of downburst events, and related parameters, will be obtained and the statistical analysis of these parameters will enable to perform long term Monte Carlo simulation on downburst events to create, for each parameter, the associated extreme value distribution. These distributions will be used by engineers in the design process for the correct evaluation of downburst wind loading on structures. For example, it will be possible to express the maximum downburst wind velocity as a function of the mean return period, which is a key issue of structural safety and sustainability. On the other hand, the authors will continue studying the uncertainties related to the parameters found using the TLBO algorithm for each downburst reconstruction. Since the algorithm is stochastic, it is possible to perform a large number of independent runs of a single downburst event and study the variability of the 11 parameters related to the analytical model from a statistical point of view.

Eqs. 113

Author contributions

The paper is part of the Ph.D. thesis of Andi Xhelaj whose supervisors are Prof. Giovanni Solari and Prof. Massimiliano Burlando. Andi Xhelaj conceptualized the study and methodology, organized the data,

performed data analysis, prepared the manuscripts and figures. Prof. Massimiliano Burlando supervised the study and made the first review. This gave rise to an iterative process leading to the final version of the paper.

Declaration of Competing Interest

The authors declare that they have no known competing financial interests or personal relationships that could have appeared to influence the work reported in this paper.

Acknowledgments

This research is funded by the European Research Council (ERC) under the European Union's Horizon 2020 Research and Innovation Program (Grant agreement No. 741273) for the project THUNDERR – Detection, simulation, modelling and loading of thunderstorm outflows to design wind-safer and cost-efficient structures – supported by an Advanced Grant 2016. The data used for this research was recorded by the monitoring network set up as part of the European Projects Winds and Ports (grant No. B87E09000000007) and Wind, Ports and Sea (grant No. B82F13000100005), funded by the European Territorial Cooperation Objective, Cross-border program Italy-France Maritime 2007-2013.

The authors are deeply grateful to Prof. Giovanni Solari for his essential contribution to the conceptualization of this research.

Appendix A

In the current appendix the calculation of Relative Wind Speed and Direction Error is explained in detail. As far as the Relative Wind Speed Error $F_{WS}(\boldsymbol{X})$ is concerned, let $\boldsymbol{V}_O(\boldsymbol{X}) = \{V_{O1}V_{O2}\ldots V_{ON}\}$ be the set of simulated wind speed data at the observing point O in $\Delta t = 1$ h and let $\boldsymbol{V} = \{V_1V_2\ldots V_N\}$ be the set of data points of the recorded wind speed for $\Delta t = 1$ h. N is the total sample of simulated wind speed data in 1 h. Since the simulation time step in this work is assumed to be $\Delta t_S = 1$ s, then $N = 3600$. The Relative Error between simulated and recorded wind speed data is defined as follows:

$$F_{WS}(\boldsymbol{X}) = \frac{\| \boldsymbol{V}_O(\boldsymbol{X}) - \boldsymbol{V} \|_2^2}{\| \boldsymbol{V} \|_2^2} \tag{A1}$$

Where $\| \cdot \|_2$ is the l_2 (Euclidean) norm of a vector, $\| \boldsymbol{V} \|_2 = \sqrt{\sum_{i=1}^{N} V_i^2}$. In Eq. (A1) the numerator is the square of the Wind Speed Error. So, the Relative Wind Speed Error is defined as the normalization of the square of the Absolute Error with the norm squared of the recorded wind speed. Applying the definition of the l_2 norm Eq. (A1) becomes:

$$F_{WS}(\boldsymbol{X}) = \frac{\sum_{i=1}^{N} (V_{Oi}(\boldsymbol{X}) - V_i)^2}{\sum_{i=1}^{N} V_i^2} \tag{A2}$$

As for the Relative Wind Direction Error $F_{WD}(\boldsymbol{X})$, its definition is less trivial than the Relative Wind Speed Error, since wind direction is a circular data with a discontinuity in $\alpha = 360°$. This is the reason why $F_{WD}(\boldsymbol{X})$ cannot be computed as $F_{WS}(\boldsymbol{X})$. To overpass this issue a polar to rectangular mapping is introduced for each simulated and recorded wind direction data: $\alpha_{Oi}(\boldsymbol{X}) \Leftrightarrow \boldsymbol{r}_{Oi}(\boldsymbol{X}) = (x_{Oi}(\boldsymbol{X}), y_{Oi}(\boldsymbol{X})) = (-\sin(\alpha_{Oi}(\boldsymbol{X})), -\cos(\alpha_{Oi}(\boldsymbol{X})))$ and $\alpha_i \Leftrightarrow \boldsymbol{r}_i = (x_i, y_i) = (-\sin(\alpha_i), -\cos(\alpha_i))$, with $i = 1, 2, \ldots, N$ (Fig. A1). Eq. A2

After this transformation it is possible to define the Relative Wind Direction Error following the same pattern of Eq. (A1):

$$F_{WD}(\boldsymbol{X}) = \frac{\sum_{i=1}^{N} \| \boldsymbol{r}_{Oi}(\boldsymbol{X}) - \boldsymbol{r}_i \|_2^2}{\sum_{i=1}^{N} \| \boldsymbol{r}_i \|_2^2} \tag{A3}$$

The numerator of Eq. (A3) represents the square of the Wind Direction Error; after expanding the numerator using the definition of the l_2 Norm and noting that $\sum_{i=1}^{N} \| \boldsymbol{r}_i \|_2^2 = \sum_{i=1}^{N} [\sin^2(\alpha_i) + \cos^2(\alpha_i)] = N$, Eq. (A3) becomes:

$$F_{WD}(\boldsymbol{X}) = \frac{1}{N} \cdot \sum_{i=1}^{N} \left\{ [\sin(\alpha_i) - \sin(\alpha_{Oi}(\boldsymbol{X}))]^2 + [\cos(\alpha_i) - \cos(\alpha_{Oi}(\boldsymbol{X}))]^2 \right\} \tag{A4}$$

Finally, after expanding Eq. (A4) and using the trigonometric formula: $\cos(\alpha_i - \alpha_{Oi}(\boldsymbol{X})) = \sin(\alpha_i) \cdot \sin(\alpha_{Oi}(\boldsymbol{X})) + \cos(\alpha_i) \cdot \cos(\alpha_{Oi}(\boldsymbol{X}))$ Eq. (A4) becomes:

$$F_{WD}(\boldsymbol{X}) = \frac{2}{N} \cdot \sum_{i=1}^{N} \{1 - cos(\alpha_i - \alpha_{Oi}(\boldsymbol{X}))\} \tag{A5}$$

The normalization of the Wind Speed and Direction Error is needed in the construction of the Objective Function in order to combine together the Relative Wind Speed and Direction Error. Eq. A5

Appendix B

The following appendix provides a detailed analysis of the fact that the uncertainty associated with the anemometric measurements has no impact on the uncertainties associated with the model predictions. All the anemometers used in the current study have a sampling rate of 10 Hz and an accuracy range of ± 0.01 m/s for the wind speed and ± 1° for the wind direction. Considering the uncertainty in the wind velocity, it is worth mentioning that for downburst reconstruction/simulation, only the 30 second moving average time histories of the wind speed and direction have been used. The moving average operator denoise the original signal and consequently reduce the error present in the measurements. Assuming that the measured wind velocity at the generic i-th sample is $V_m[i]$ and the correct velocity is $V_c[i]$, it is possible to assume that $V_m[i] = V_c[i] + e[i]$, where $e[i]$ is the instantaneous error present in the i-th measurement; e is a random error and therefore can be viewed as an outcome of a random variable E with a specified distribution. This means that each occurrence $e[i]$ can be viewed as the outcome of the corresponding random variable $E[i]$, with $i = 1, 2, \ldots, N$, where N is the length of the measured signal and is equal to $N = 36000$ samples (i.e., 1 hour time history sampled at 10 Hz). Assuming the independence of errors it is possible to model the random variables $E[i]$, $i = 1, \ldots, N$, as independent and identically distributed. Applying the 30 second

moving average operator to $V_m[i]$ it can be shown that the measured moving average wind velocity is given by $\overline{V_m}[i] = \overline{V_c}[i] + \overline{e}[i]$, where $\overline{e}[i] = \frac{1}{M}\sum_{k=1}^{M} e[i+k]$ with $i = 1, 2, \ldots, N - M$. In this case, the forward moving average operator is considered. M is the number of samples present in 30 seconds and so is equal to $M = 300$. Following the same reasoning as above, the i-th occurrence $\overline{e}[i]$ can be viewed as the outcome of the random variable $\overline{E}[i] = \frac{1}{M}\sum_{i=1}^{M} E[i+k]$. To assess the uncertainty present in the measured moving average wind speed it is important to evaluate the distribution of the random variables $\overline{E}[i]$. According to the Central Limit Theorem (CLT), the probability distribution of the sum of M independent identically distributed random variables tend to become Gaussian for large values of M. Assuming that $E[i]$ is a zero mean random variable with standard deviation σ, then $\overline{E}[i]$ for $M \to \infty$ will tend to have a Gaussian distribution with zero mean and standard deviation $\overline{\sigma} = \frac{\sigma}{\sqrt{M}} \to 0$, which means that in the limit case, the dispersion of the uncertainty when considering the measured moving average wind velocity will tend to zero; in this way the moving average operator denoise the signal reducing the error present in the measurements.

From the numerical standpoint, assuming for example that all the random variables $E[i]$ are uniformly distributed in $-0.01 \le e \le 0.01$ m/s, which is the accuracy range of the ultrasonic anemometer, then, the standard deviation of the random variables $E[i]$ will be $\sigma = 0.01/\sqrt{3} = 0.005774$ m/s. Then, if $M = 32$ it is possible to show that the probability density function of $\overline{E}[i]$ is almost identical to the Gaussian probability density function, and for $M = 300$ the approximation perfectly converges to the Gaussian probability density function. Therefore, it is possible to say that all the random variables $\overline{E}[i]$ have a normal distribution with zero mean and variance $\overline{\sigma} = \frac{\sigma}{\sqrt{M}} = \frac{0.01}{\sqrt{3 \cdot M}} = 0.000333$ m/s. This result ensures that 99.7 % of the outcomes $\overline{e}[i]$ will be in the range:

$-3 \cdot \overline{\sigma} \le \overline{e}[i] \le 3 \cdot \overline{\sigma}$ or $-0.001 \le \overline{e}[i] \le 0.001$ m/s. So, the error is in the order of mm/s and can be completely ignored since the uncertainty is very low. Thus, it is possible to assume that the measured moving average wind velocity $\overline{V_m}[i]$ coincides with the correct moving average wind velocity $\overline{V_c}[i]$. The same result holds for the horizontal wind components, namely $\overline{V_{mx}}[i] = \overline{V_{cx}}[i]$ and $\overline{V_{my}}[i] = \overline{V_{cy}}[i]$, and consequently it is possible to extend the result to the moving average wind direction. These results indicate that the error in the measurement has very small impact on the uncertainties associated with the model predictions.

References

[1] Letchford CW, Mans C, Chay MT. Thunderstorms – their importance in wind engineering (a case for the next generation wind tunnel). J Wind Eng Ind Aerodyn 2002;90:1415–33.
[2] Solari G. Emerging issues and new frameworks for wind loading on structures in mixed climates. Wind Struct 2014;19:295–320.
[3] Fujita TT. Tornadoes and downbursts in the context of generalized planetary scales. J Atmos Sci 1981;38:1511–34.
[4] Fujita TT. Downburst: microburst and macroburst. Univ Chic Press 1985;II:122.
[5] Fujita TT. Downburst: meteorological features and wind field characteristics. J Wind Eng Ind Aerodyn 1990;36:75–86.
[6] Fujita TT, Wakimoto RM. Five scales of airflow associated with a series of downbursts on 16 July 1980. Mon Weather Rev 1981;109:1438–56.
[7] Davenport AG. The application of statistical concepts to the wind loading of structures. P I Civ Eng 1961;19:449–72.
[8] Xhelaj A, Burlando M, Solari G. A general-purpose analytical model for reconstructing the thunderstorm outflows of travelling downbursts immersed in ABL flows. J Wind Eng Ind Aerodyn 2020;207:104373.
[9] Solari G, Repetto MP, Burlando M, De Gaetano P, Pizzo M, Tizzi M, Parodi M. The wind forecast for safety and management of port areas. J Wind Eng Ind Aerodyn 2012;104-106:266–77.
[10] Repetto MP, Burlando M, Solari G, De Gaetano P, Pizzo M. Integrated tools for improving the resilience of seaports under extreme wind events. Sustain Cities Soc 2017;32:277–94.
[11] Repetto MP, Burlando M, Solari G, De Gaetano P, Pizzo M, Tizzi M. A web-based GIS platform for the safe management and risk assessment of complex structural and infrastructural systems exposed to wind. Adv Eng Software 2018;117:29–45.
[12] Burlando M. Downburst outflow reconstruction by wind profile measurements. In: Proceedings of the 15th International Conference on Wind Engineering; 2019, A092704. September 1-6 Beijing, China.
[13] Zhang S, Solari G, Burlando M, Yang Q. Directional decomposition and properties of thunderstorm outflows. J Wind Eng Ind Aerodyn 2019;189:71–90.
[14] Burlando M, Zhang S, Solari G. Monitoring, cataloguing, and weather scenarios of thunderstorm outflows in the northern Mediterranean. Nat Hazards Earth Sci 2018; 18:2309–30.
[15] Burlando M, Romanic D, Solari G, Hangan H, Zhang S. Field data analysis and weather scenario of a downburst event in Livorno, Italy on 1 October 2012. Mon Weather Rev 2017;145:3507–27.
[16] Solari G, Burlando M, De Gaetano P, Repetto MP. Characteristics of thunderstorms relevant to the wind loading of structures. Wind Struct 2015;20:763–91.
[17] Solari G. Thunderstorm downburst and wind loading of structures: progress and prospect. Front Built Environ 2020.
[18] Hjelmfelt MR. Structure and life cycle of microburst outflows observed in Colorado. J Appl Meteorol 1988;27:900–27. August.
[19] Holmes JD, Oliver SE. An empirical model of a downburst. Eng Struct 2000;22: 1167–72.
[20] Chay MT, Albermani F, Wilson B. Numerical and analytical simulation of downburst wind loads. Eng Struct 2006;28:240–54.
[21] Hjelmfelt MR. The Microburst of 22 June 1982 in JAWS. J Atmos Sci 1987;44(12).
[22] Glover F, Kochenberger GA. Handbook of Metaheuristics. Springer; 2003.
[23] Glover F. Future paths for integer programming and links to artificial intelligence. Comput Operat Res 1986;13:533–49.
[24] Bianchi L, Dorigo M, Gambardella LM, Gutjahr WJ. A survey on metaheuristics for stochastic combinatorial optimization. Nat Comput 2009;8(2):239–87.
[25] Holland J. Adaptation in Natural and Artificial Systems. Ann Arbor: University of Michigan Press; 1975.
[26] Kirkpatrick S, Gelatt CD, Vecchi MP. Optimization by simulated annealing. Science 1983;220(4598):671–80.
[27] Glover F, Laguna M. Tabu Search. Boston: Kluwer; 1997.
[28] Dorigo M. PhD thesis. in Italian. Milan, Italy: Dipartimento di Elettronica, Politecnico di Milano; 1992.
[29] Kennedy J, Eberhart R. Particle swarm optimization. In: Proceedings of the IEEE International Conference on Neural Networks. IV; 1995. p. 1942–8.
[30] Geem ZW, Kim JH, Loganathan GV. A new heuristic optimization: harmony search. Simulation 2001;76:60–8.
[31] Karaboga D., 2005. An idea based on honey bee swarm for numerical optimization. Technical report TRo6, Erciyes University, Turkey.
[32] Yang XS, Deb S. Cuckoo Search via Lévy flights. In: Proceedings of the 2009 World Congress on Nature & Biologically Inspired Computing (NaBIC); 2009. p. 210–4.
[33] Storn R, Price K. Differential evolution - a simple and efficient heuristic for global optimization over continuous spaces. J Global Optimizat 1997;11(4):341–59.
[34] Rao RV, Savsani VJ, Vakharia DP. 'Teaching–learning-based optimization: a novel method for constrained mechanical design optimization problems'. Comput-Aided Des 2011;43(3):303–15.
[35] Storn R. On the usage of differential evolution for function optimization. In: Proceedings of the Biennial Conference of the North American Fuzzy Information Processing Society (NAFIPS); 1996. p. 519–23.
[36] Price K, Storn RM, Lampinen JA. Differential Evolution: A Practical Approach to Global Optimization. Springer; 2005. ISBN.
[37] Rao RV. Teaching Learning Based Optimization Algorithm and Its Engineering Applications. Springer; 2016.
[38] Wilson JW, Roberts RD, Kessinger C, McCarthy J. Microburst wind structure and evaluation of doppler radar for airport wind shear detection. J Climate Appl Meteorol 1984;23:898–915.
[39] Wilson JW, Wakimoto RM. The discovery of the downburst: T. T. Fujita's contribution. Bull Amer Meteorol Soc 2001;82:49–62.
[40] Kim J, Hangan H. Numerical simulations of impinging jets with application to downbursts. J Wind Eng Ind Aerodyn 2007;95:279–98.
[41] Xu Z, Hangan H. Scale, boundary and inlet condition effects on impinging jets. J Wind Eng Ind Aerodyn 2008;96:2383–402.
[42] Mason MS, Wood GS, Fletcher DF. Numerical simulation of downburst winds. J Wind Eng Ind Aerodyn 2009;97:523–39.
[43] Zaharie D. Critical values for the control parameters of differential evolution algorithms. In: Proceedings of the 8th International Conference on Soft Computing (MENDEL). Brno, Czech Republic; 2002. p. 62–7.